Continental Lower Crust

Bradley R. Hacker,[1] Peter B. Kelemen,[2] and Mark D. Behn[3]

[1]Department of Earth Science, University of California, Santa Barbara, California 93106; email: hacker@geol.ucsb.edu

[2]Department of Earth and Environmental Sciences, Lamont-Doherty Earth Observatory, Columbia University, Palisades, New York 10964; email: peterk@ldeo.columbia.edu

[3]Department of Geology and Geophysics, Woods Hole Oceanographic Institution, Woods Hole, Massachusetts 02543; email: mbehn@whoi.edu

Annu. Rev. Earth Planet. Sci. 2015. 43:167–205

First published online as a Review in Advance on February 20, 2015

The *Annual Review of Earth and Planetary Sciences* is online at earth.annualreviews.org

This article's doi: 10.1146/annurev-earth-050212-124117

Keywords

continental crust, relamination, delamination, lower crust, differentiation, wavespeeds, heat flow

Abstract

The composition of much of Earth's lower continental crust is enigmatic. Wavespeeds require that 10–20% of the lower third is mafic, but the available heat-flow and wavespeed constraints can be satisfied if lower continental crust elsewhere contains anywhere from 49 to 62 wt% SiO_2. Thus, contrary to common belief, the lower crust in many regions could be relatively felsic, with SiO_2 contents similar to andesites and dacites. Most lower crust is less dense than the underlying mantle, but mafic lowermost crust could be unstable and likely delaminates beneath rifts and arcs. During sediment subduction, subduction erosion, arc subduction, and continent subduction, mafic rocks become eclogites and may continue to descend into the mantle, whereas more silica-rich rocks are transformed into felsic gneisses that are less dense than peridotite but more dense than continental upper crust. These more felsic rocks may rise buoyantly, undergo decompression melting and melt extraction, and be relaminated to the base of the crust. As a result of this refining and differentiation process, such relatively felsic rocks could form much of Earth's lower crust.

INTRODUCTION

Characterizing the composition of Earth's lower crust and understanding the physical and chemical processes that produced its characteristics are relevant to geodynamics, geochemistry, and seismology. For example, in geodynamics, we seek to understand where, why, and at what timescales and lengthscales body forces evolve. In geochemistry, we investigate how physical and chemical processes have shaped the differentiation of Earth's crust—for example, how radiogenic is lower crust? In seismology, we evaluate the constraints that wavespeeds provide about the composition of Earth's lower crust.

This manuscript builds on earlier reviews concerning continental crust (e.g., McLennan et al. 2005; Rudnick & Gao 2003, 2014), focusing on three questions specific to continental lower crust:

1. What is the composition of continental lower crust?
2. What major processes change the composition of lower continental crust?
3. What are the mechanisms and rates of continental crust recycling?

We begin by reviewing the compositions of lower crustal granulite- and amphibolite-facies terrains and continental granulite xenoliths, followed by the constraints on lower crust composition afforded by heat-flow and seismic wavespeed data sets. We conclude that Earth's crust is well described as a two-layer felsic crust in some tectonic settings and as a three-layer crust with a thin mafic lower crust in other settings. We then discuss proposed crustal differentiation and recycling mechanisms, emphasizing the potential importance of relamination.

THICKNESS, LAYERING, AND COMPOSITION OF CONTINENTAL CRUST

Earth's continental crust is widely believed to be andesitic to dacitic, with 57 to 66 wt% SiO_2 (e.g., Rudnick & Gao 2003, 2014), distinct from mafic oceanic crust, with 48 to 52 wt% SiO_2, and from upper mantle residual peridotites, with <46 wt% SiO_2. Compared with oceanic crust and upper mantle, continental crust has slower seismic wavespeeds and is less dense (Holbrook et al. 1992, Rudnick & Fountain 1995). How and when these attributes developed is understood in general, but not specific, terms. There is great variety in the chemical and physical properties within the crust—for example, the differences between Earth's sedimentary veneer and the crystalline rocks exhumed from the lower crust. There are also differences in the thickness of continental crust—and the nature of the Mohorovičić (Moho) discontinuity—in different tectonic settings. Whether these downward changes in physical and chemical properties occur gradually or in distinct layers of regional significance is not well known.

Crustal Thickness

The release of considerable new seismic-refraction data from Russia and China in the early 1990s prompted reexamination of the thicknesses and wavespeeds of continental crust (e.g., Mooney et al. 1998). Crustal thickness varies considerably with tectonic setting, but the average crust was determined to be ~40 km thick (**Figure 1*a***) (Christensen & Mooney 1995, Rudnick & Fountain 1995). Recently, Huang et al. (2013) calculated a thinner average crustal thickness from the 2° × 2° CRUST2.0 wavespeed–thickness model (Bassin et al. 2000)—principally because CRUST2.0 includes substantially more submerged continental crust. They then merged that with global gravity data (suggesting 32.7 km) and surface-wave dispersion data (34.8 km) to yield an average crustal thickness of 34.4 ± 4.1 km (**Figure 1*b***). The most recent wavespeed–thickness

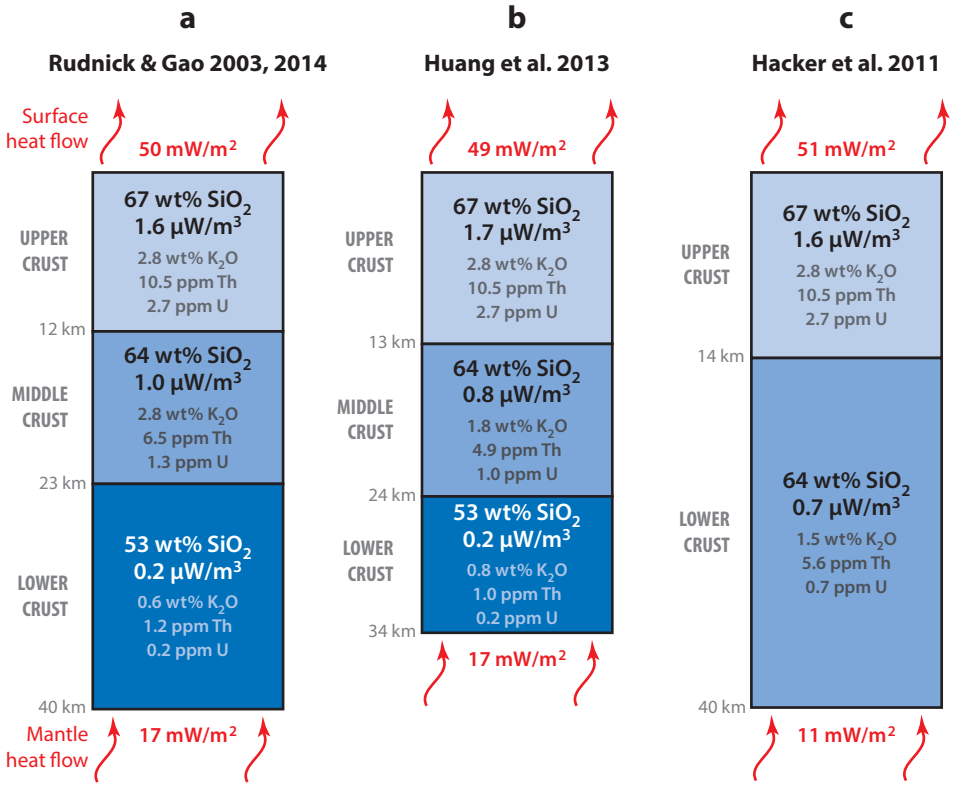

Figure 1

(*a*) Rudnick & Gao's (2003, 2014) three-layer crustal model uses a mantle heat flow of 17 mW/m^2, the measured composition of upper crust, a middle crust composition from post-Archean granulite-facies terrains, lower crustal wavespeeds, and the compositions of xenoliths to conclude that lower crust is 80% mafic and 17 km thick. (*b*) Huang et al. (2013) used a newer seismic data set to infer a 10-km-thick, mafic lower crust. (*c*) Hacker et al. (2011) used a lower (11 mW/m^2) bound on mantle heat flow (Michaut et al. 2009) to show that a two-layer crust with no mafic rock is possible.

model—the 1° × 1° CRUST1.0 (Laske et al. 2013) model (**Table 1**)—is not substantively different from CRUST2.0 and does not change the 34.4-km thickness calculated by Huang et al. (2013).

Crustal Layers

Earth's continental crust has been divided into two to four layers—termed upper, middle, lower, and/or lowermost crust—on the basis of seismic wavespeeds (**Figure 1**). These layers may have clear geologic meaning at specific locations—for example, a large sedimentary basin may constitute an upper crustal layer with distinct wavespeeds. In general, however, seismically defined deeper crustal layers may be model artifacts, not regionally extensive, or caused by different features from point to point. The velocity structure of the crust is just as likely a gradient punctuated throughout by faster or slower layers of variable thickness (Bond et al. 2007, Smithson 1978). The presence of seismically distinct layers is not a universal feature of continental crust, and interpretation of such layers should be done with caution.

Table 1 Thickness of continental crust layers from CRUST1.0

Tectonic setting	Area (%)	Upper crust (km)	Middle crust (km)	Lower crust (km)	Entire crust (km)
Shields and platforms	49	13.7	13	12.1	38.8
Rifts, sensu lato	11	11.4	10.6	10.6	32.6
Orogens, Paleozoic–Mesozoic	11	15.8	13.9	10	39.7
India-Asia collision zone	4	26.2	12.2	13.3	51.7
Continental shelf*	10	13.2	9.5	8.9	31.6
Continental slope*	7	6.8	6.1	10.2	23.1
Margin-continent transition*	6	11.1	9.3	9.6	30.0
Oceanic continental plateau*	2	6.5	5.1	5.4	17.0
Whole crust (average)	**100**	**13.5**	**11.7**	**10.9**	**36.1**

Cenozoic noncollisional orogens, continental margins, and inland seas are not included. Asterisks denote submerged settings.

In spite of these limitations, layers are widely used in the literature to describe crust. Rudnick & Gao (2003, 2014), for example, used upper, middle, and lower crustal layers with thicknesses of 12, 11, and 17 km, respectively, following from their previous work (Gao et al. 1998, after Rudnick & Fountain 1995). The CRUST1.0 model yields areally weighted average thicknesses of 13.5, 11.7, and 10.9 km for upper, middle, and lower crust, respectively (**Table 1**).

Composition of Lower Crust

The composition and physical properties of upper continental crust are reasonably well known from outcrops and fine-grained clastic sediment (Rudnick & Gao 2003, 2014, and references therein). The compositions of middle and lower crust are more difficult to determine and are estimated from exposed terrains recording lower crustal pressures, xenoliths, and geophysical data. In their influential reviews, Rudnick & Gao (2003, 2014) chose a composition for middle crust by averaging mid-crustal rocks exposed in China (Gao et al. 1998) plus worldwide granulite-facies terrains whose compositions were corrected for K, U, Th, and Pb depletion (Rudnick & Fountain 1995). They then inferred that lower crust is 80% mafic (53 wt% SiO_2), based on (*i*) the compositions of granulite-facies terrains and xenoliths erupted from lower crust, (*ii*) the inferred heat flow from lower crust, and (*iii*) lower crustal seismic wavespeeds (**Figure 1*a***). Huang et al. (2013) updated this approach to more fully constrain the K, U, and Th contents of these layers, and inferred the composition of middle crust from amphibolite-facies terrains (**Figure 1*b***). By contrast, Hacker et al. (2011) used a two-layer model that also fit the available geophysical constraints to demonstrate that lower crust might not be mafic (**Figure 1*c***).

Granulite- and amphibolite-facies terrains. The composition of deeply exhumed, granulite-facies terrains has been used since the 1960s (e.g., Heier & Adams 1965, Lambert & Heier 1968, Shaw et al. 1967) to infer the composition of lower crust. There are many metamorphic terrains that record peak pressures of 0.8 to 1.2 GPa, corresponding to lower crustal depths in cratons and mid-crustal levels of orogenic plateaux. Only one such granulite terrain, the Ivrea zone, is contiguous with mantle rock—and, therefore, clearly lowermost crust. Geophysical data suggest that others (e.g., Kapuskasing, Vredefort) may be immediately underlain by mantle (Fountain & Salisbury 1981, Percival et al. 1992, Tredoux et al. 1999).

To characterize the composition of continental granulite-facies terrains, Rudnick & Presper (1990) assembled a database of rock compositions from Archean and post-Archean terrains recrystallized at >0.6 GPa. Huang et al. (2013) updated this database and added a compilation of amphibolite-facies samples. We augmented their granulite data with additional analyses from the literature, and here we draw conclusions from the augmented data set (**Figure 2**, **Table 2**, and **Supplemental Tables 1** and **2**; follow the **Supplemental Material link** in the online version of this article or at **http://www.annualreviews.org/**); we use median values for major elements, normalized to 100%, and log-normal average (exp{average[ln(x_1, x_2. . .x_n)]}) values for trace elements. Only a small fraction of geochemical studies of granulite terrains have been done in a systematic manner (e.g., with gridded sample locations or by weighting individual analyses by exposure area), so the database is mainly composed of samples said to be representative or chosen for some particular reason (e.g., study of charnockite formation). This has caused an unquantifiable skewing of the database. A time-consuming but useful addition to our knowledge would be true grid sampling of key granulite terrains.

Supplemental Material

The updated database of Archean granulite-facies terrains (**Table 2**) shows minor differences from Rudnick & Presper's (1990) values (also normalized to 100%). The new composition for Archean terrains has 10–20% more Mg, Sc, Ni, and Cu; 10–30% less rare earth elements (REEs), Sr, Y, Zr, Nb, and Ba; and 20–40% less Rb, Hf, Ta, Th, and U; the reduced trace-element concentrations are amplified by our choice of log-normal average, rather than median, values. This results in a heat-production rate of 0.36 $\mu W/m^3$ (**Supplemental Table 3**), 25% less than reported by Rudnick & Presper (1990). [We follow Rudnick & Presper (1990) and Huang et al. (2013) in excluding X-ray fluorescence measurements of Th and U.]

The new composition for post-Archean granulite terrains also is somewhat different from the median composition determined by Rudnick & Presper (1990). The new composition has 10–20% more Mn, Mg, Ca, Cr, Ni, and Cu; 10–20% less Sc, Ga, and Ba; 20–40% less Co, Zn, Rb, Y, Zr, REEs, and U; and 70% less Nb and Th. This results in a 40% lower heat-production rate of 0.41 $\mu W/m^3$ (the rate in table 4 of Rudnick & Presper 1990 should read 0.69 $\mu W/m^3$, rather than 0.53 $\mu W/m^3$).

The updated database preserves the general differences between Archean and post-Archean terrains noted by Rudnick & Presper (1990): The younger terrains are enriched relative to the older terrains in Fe, Mg, Ca, P, Ti, Sc, V, middle rare earth elements (MREEs), heavy rare earth elements (HREEs), Hf, Ta, and U and depleted in Si and some large-ion lithophile elements, including K, Pb, and Th. Both are quite silica rich: 69 and 64 wt% (dacitic or granodioritic).

The compilation of amphibolite-facies metamorphic terrains (Huang et al. 2013) has median and log-normal average values similar to those of post-Archean granulites, with 64 wt% SiO_2, but has higher MREEs, HREEs, Li, Rb, Cs, U, and Th. **Figure 3** shows that the median and log-normal average amphibolite-facies rock composition falls within the range of estimates for bulk continental crust for an extensive suite of major and trace elements, whereas the granulite terrains and xenoliths are significantly depleted in Ta, U, and Th compared with bulk continental crust.

It is evident from **Figure 2** that describing the data with a single median or log-normal average value masks richness in the data. The SiO_2 values from Archean granulites are bimodal, perhaps reflecting the bimodal mafic (greenstone)–felsic (granitoid) association often said to be characteristic of the Archean (e.g., Barker & Peterman 1974). The SiO_2 values from amphibolite-facies and post-Archean granulite-facies rocks also show a bimodal distribution, and they include a larger number of mafic rocks than the compilation of samples from Archean terrains. K_2O and Th are markedly enriched in silica-rich compositions (69–79 wt% SiO_2) compared with more mafic compositions (48–56 wt% SiO_2), whereas U is less so. These values reflect the fact that the compiled compositions of samples from both Archean and post-Archean granulite-facies terrains include a

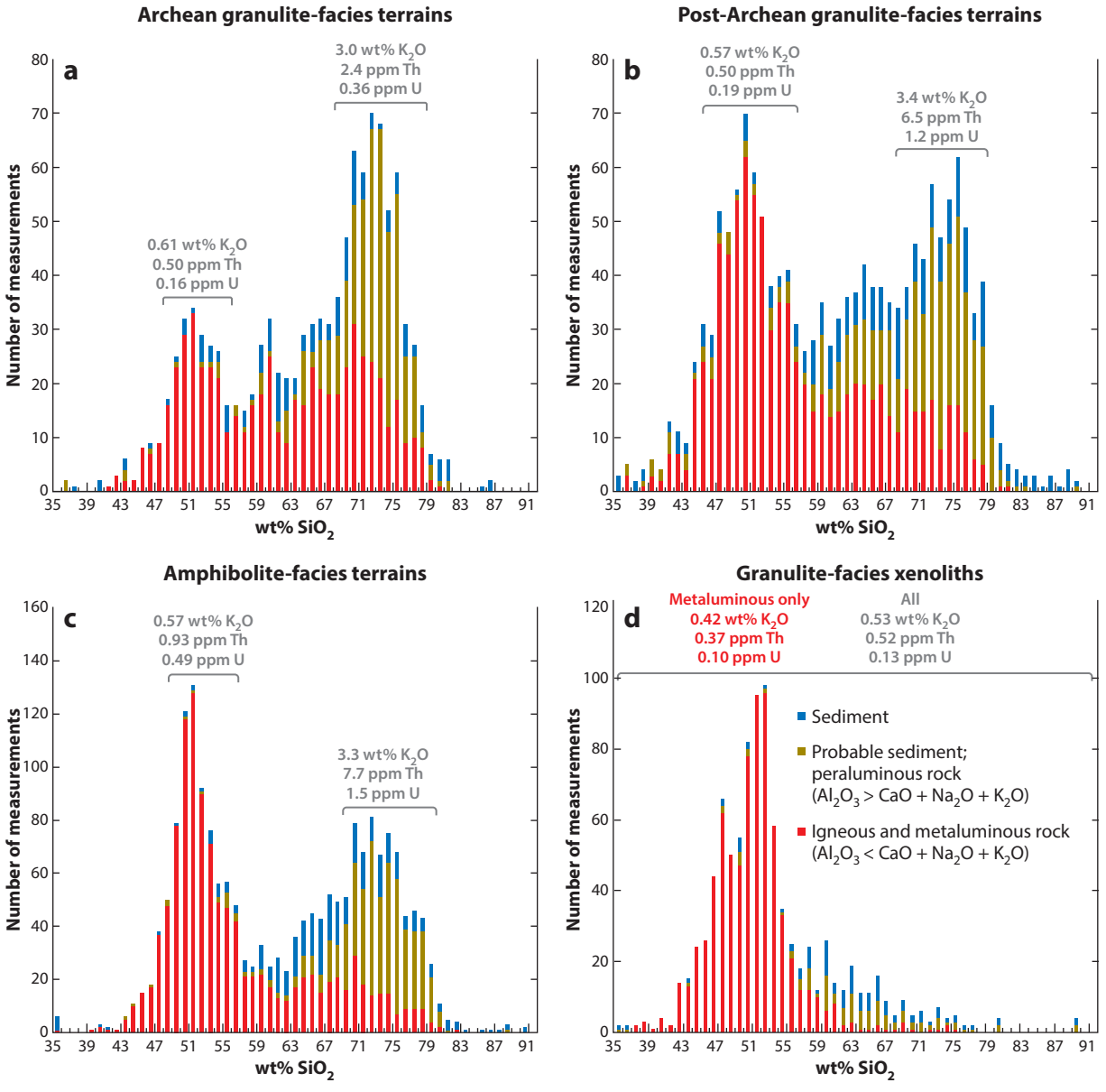

Figure 2

SiO_2 histograms for possible lower crustal rocks; K, Th, and U median values are shown for 48–56 and 68–79 wt% SiO_2. (*a*) Archean granulite-facies rocks have bimodal compositions; 13% are metasedimentary, and the 44% that are peraluminous may be metasedimentary. (*b*) Post-Archean granulite-facies rocks are more mafic and more radiogenic; 17% are metasedimentary, and 44% may be metasedimentary. (*c*) Amphibolite-facies terrains are very similar. (*d*) Granulite-facies xenoliths are dominated by rather unradiogenic mafic rocks; 9% are metasedimentary, and 16% may be metasedimentary.

Table 2 Compositions of terrains and xenoliths

	Archean granulite-facies terrains[1]					Post-Archean granulite-facies terrains[1]					Amphibolite-facies terrains[2]					Deep crustal xenoliths[2]				
	n	*mdn*	*avg*	*SD*	ln(*avg*)	*n*	*mdn*	*avg*	*SD*	ln(*avg*)	*n*	*mdn*	*avg*	*SD*	ln(*avg*)	*n*	*mdn*	*avg*	*SD*	ln(*avg*)
SiO_2 (wt%)	1,074	**68.7**	64.1	11.5	61.4	1,652	**64.2**	60.8	12.9	58.3	1,835	**63.8**	61.4	10.6	60.1	1,001	**52.1**	52.4	7.3	51.7
TiO_2 (wt%)	1,058	**0.5**	0.6	0.4	0.4	1,614	**0.7**	0.8	0.7	0.5	1,835	**0.7**	0.9	0.8	0.6	998	**0.9**	1.1	0.8	0.8
Al_2O_3 (wt%)	1,071	**15.2**	14.6	3.5	13.7	1,571	**15.9**	15.4	4.6	14.1	1,835	**15.6**	15.1	2.8	14.6	1,001	**17.0**	16.5	4.0	15.9
FeO^T (wt%)	1,073	**4.6**	5.8	4.8	4.2	1,571	**6.7**	7.0	4.3	5.4	1,835	**6.7**	7.1	4.7	5.4	1,001	**9.0**	9.1	3.5	8.3
MnO (wt%)	1,003	**0.07**	0.10	0.10	0.07	1,555	**0.11**	0.12	0.10	0.09	1,825	**0.13**	0.13	0.10	0.10	980	**0.15**	0.17	0.40	0.14
MgO (wt%)	1,066	**2.0**	3.8	5.4	1.8	1,570	**3.3**	4.9	6.1	2.5	1,833	**3.2**	4.1	3.8	2.3	1,001	**7.3**	7.7	4.2	6.4
CaO (wt%)	1,073	**3.6**	5.3	5.9	3.5	1,570	**4.7**	5.9	5.6	3.3	1,835	**4.8**	5.9	4.5	3.9	1,001	**10.3**	9.4	4.0	8.0
Na_2O (wt%)	1,067	**3.6**	3.3	1.4	2.6	1,561	**2.9**	2.8	1.5	2.1	1,832	**3.3**	3.1	1.3	2.7	1,001	**2.6**	2.6	1.3	2.2
K_2O (wt%)	1,176	**1.7**	2.2	1.8	1.4	1,710	**1.4**	2.1	2.1	1.1	1,618	**1.6**	2.0	1.6	1.2	996	**0.5**	0.9	1.0	0.5
P_2O_5 (wt%)	1,006	**0.10**	0.20	0.50	0.10	1,444	**0.14**	0.21	0.30	0.12	1,805	**0.13**	0.16	0.20	0.11	954	**0.13**	0.20	0.30	0.12
K (ppm)	1,176	13,390	18,175	14,716	11,709	1,710	11,152	17,048	17,212	8,827	1,833	13,094	16,801	13,717	10,267	996	4,313	7,380	8,503	4,053
Ti (ppm)	1,058	2,995	3,433	2,473	2,538	1,614	3,981	4,944	4,237	3,290	1,835	4,110	5,224	4,496	3,634	998	5,281	6,311	4,667	4,845
Li (ppm)	64	12	18	27	**12**	47	6	7	5	**5**	418	15	20	38	**14**	127	6	7	5	**5**
Sc (ppm)	361	11	16	15	**9**	475	24	26	16	**20**	1,131	18	22	16	**15**	576	29	31	16	**27**
V (ppm)	694	73	102	100	**57**	1,063	117	147	130	**85**	1,632	119	158	140	**88**	731	187	213	137	**169**
Cr (ppm)	742	61	222	588	**56**	1,065	62	231	583	**63**	1,517	67	171	431	**53**	798	151	281	413	**145**
Co (ppm)	361	23	35	35	**20**	718	20	31	33	**16**	1,145	26	31	26	**19**	499	41	47	34	**39**
Ni (ppm)	734	30	101	263	**32**	1,116	26	101	373	**28**	1,524	35	65	129	**26**	785	86	125	130	**81**
Cu (ppm)	521	14	30	58	**15**	729	15	35	48	**18**	1,065	22	46	76	**21**	564	35	57	118	**34**
Zn (ppm)	624	59	65	51	**49**	936	67	77	78	**55**	1,344	77	93	157	**70**	530	86	90	47	**78**
Ga (ppm)	515	18.0	18.6	6.1	**17.5**	776	18.3	18.9	9.1	**16.4**	932	18.4	19.4	9.5	**17.8**	274	18.0	18.0	5.3	**17.4**
Rb (ppm)	978	39	57	63	**26**	1,377	35	65	85	**23**	1,695	50	73	75	**36**	831	7	20	30	**7**
Sr (ppm)	980	268	334	361	**220**	1,419	218	342	488	**194**	1,797	201	263	212	**186**	866	413	506	432	**381**
Y (ppm)	794	16	25	34	**14**	1,214	22	30	33	**20**	1,677	23	27	19	**22**	709	18	22	18	**16**
Zr (ppm)	892	135	178	166	**122**	1,352	123	197	392	**109**	1,766	128	160	118	**115**	762	66	103	129	**59**

(*Continued*)

Table 2 (*Continued*)

	Archean granulite-facies terrains[1]					Post-Archean granulite-facies terrains[1]					Amphibolite-facies terrains[2]					Deep crustal xenoliths[2]				
	n	*mdn*	*avg*	*SD*	ln(*avg*)	*n*	*mdn*	*avg*	*SD*	ln(*avg*)	*n*	*mdn*	*avg*	*SD*	ln(*avg*)	*n*	*mdn*	*avg*	*SD*	ln(*avg*)
Nb (ppm)	689	5	9	12	**5**	983	7	13	48	**6**	1,583	7	10	13	**7**	592	5	9	18	**5**
Cs (ppm)	164	0.4	1.2	3.5	**0.4**	483	0.3	1.4	3.2	**0.3**	654	1.3	2.5	4.3	**1.1**	216	0.1	1.0	2.1	**0.2**
Ba (ppm)	853	540	673	612	**428**	1,229	396	582	748	**305**	1,723	362	465	440	**261**	795	325	555	850	**280**
La (ppm)	696	23	33	35	**20**	1,031	17	28	42	**14**	1,585	18	26	32	**15**	696	9	15	17	**8**
Ce (ppm)	691	42	58	59	**37**	1,046	40	58	83	**31**	1,562	38	54	65	**33**	704	20	32	34	**19**
Pr (ppm)	203	5	8	10	**4**	621	4	6	7	**3**	1,081	5	7	8	**4**	346	2	4	4	**2**
Nd (ppm)	375	16	25	31	**15**	831	18	26	36	**14**	1,500	19	26	27	**18**	695	12	29	309	**12**
Sm (ppm)	452	2.8	4.3	5.6	**2.6**	805	3.9	5.2	6.3	**3.1**	1,418	4.2	5.2	4.1	**4.0**	711	3.3	4.0	3.4	**3.0**
Eu (ppm)	438	1.1	1.2	0.7	**1.0**	793	1.1	1.4	1.1	**1.0**	1,434	1.1	1.2	0.9	**1.0**	668	1.2	1.5	4.0	**1.1**
Gd (ppm)	285	3.0	4.2	4.9	**2.7**	702	3.7	4.7	4.8	**3.0**	1,270	4.0	4.8	3.3	**3.9**	452	3.4	3.9	2.7	**2.9**
Tb (ppm)	361	0.4	0.6	0.8	**0.4**	756	0.6	0.8	1.0	**0.5**	1,080	0.7	0.8	0.9	**0.6**	488	0.5	0.6	0.8	**0.4**
Dy (ppm)	309	2.8	3.8	5.2	**2.4**	651	3.5	4.1	3.4	**2.8**	1,101	4.0	4.8	3.2	**3.8**	438	3.4	4.0	3.1	**2.9**
Ho (ppm)	223	0.5	0.8	1.2	**0.4**	655	0.7	0.9	0.8	**0.6**	9,84	0.9	1.1	1.0	**0.8**	370	0.6	0.6	0.5	**0.5**
Er (ppm)	305	1.5	2.3	3.7	**1.3**	678	2.0	2.4	2.1	**1.6**	1,103	2.4	2.8	1.9	**2.2**	416	1.7	2.2	1.8	**1.5**
Yb (ppm)	435	1.2	2.0	4.0	**1.0**	797	1.9	2.5	2.9	**1.6**	1,455	2.2	2.6	1.8	**2.0**	644	1.5	2.1	2.0	**1.4**
Lu (ppm)	332	0.2	0.3	0.7	**0.2**	760	0.3	0.4	0.5	**0.3**	1,388	0.3	0.4	0.7	**0.3**	557	0.2	0.3	0.3	**0.2**
Hf (ppm)	264	2.5	2.9	2.4	**2.1**	598	3.5	5.7	13.0	**3.0**	1,178	3.5	4.6	5.4	**3.2**	420	1.7	2.8	3.4	**1.7**
Ta (ppm)	207	0.2	0.4	0.5	**0.2**	475	0.4	0.8	1.5	**0.4**	982	0.5	2.3	20.0	**0.5**	266	0.4	0.6	0.7	**0.3**
Pb (ppm)	595	11	15	16	**10**	750	10	17	46	**10**	1,168	12	16	17	**10**	443	5	9	42	**4**
Th (ppm)	426	2.1	7.9	15.8	**1.9**	672	2.0	6.6	12.3	**1.8**	712	4.5	7.3	8.2	**3.2**	384	0.3	1.8	5.1	**0.4**
U (ppm)	345	0.3	0.9	2.4	**0.3**	593	0.6	1.4	2.5	**0.6**	712	0.9	1.5	1.8	**0.8**	358	0.1	0.4	1.5	**0.1**

Major elements are normalized to 100%. Preferred values are in bold. Th and U measurements by X-ray fluorescence are excluded.
[1]Data from **Supplemental Tables 1** and **2**.
[2]Data from Huang et al. (2013).

Supplemental Material

large proportion of quartzofeldspathic gray gneiss, but post-Archean granulites also include heterogeneous mixtures of more felsic to more mafic rocks of igneous and sedimentary parentage (see references in database).

Figure 2 emphasizes that granulite and amphibolite terrains are composed of four types of rock: (*i*) gneiss that is inferred to be metasedimentary based on field relations or textures (blue); (*ii*) gneiss with unclear field relations and textures that is peraluminous [molar $Al_2O_3/(CaO + Na_2O + K_2O) > 1$] like modern pelitic sediments and therefore likely to be metasedimentary (dark yellow); (*iii*) gneiss that is inferred to be igneous on the basis of field relations or textures (red); and (*iv*) gneiss that has unclear field relations and textures but is metaluminous [molar $Al_2O_3/(CaO + Na_2O + K_2O) < 1$] like modern igneous rocks and/or immature graywackes derived from erosion of igneous rocks (also red).[1] Clearly much of the rock exposed in granulite terrains is metasedimentary, rather than igneous as commonly assumed.

Xenoliths. Granulite xenoliths from continental volcanic centers were first used systematically to infer the composition of lower crust by Rudnick and coworkers (Rudnick & Fountain 1995; Rudnick & Gao 2003, 2014; Rudnick & Presper 1990) in preference to the more-evolved samples of granulite terrains. Rudnick & Presper's (1990) xenolith database was updated by Huang et al. (2013), resulting in a new median/log-normal average xenolith composition with 20–50% more K, Cu, Ga, Rb, Zr, Cs, Nd, and Th; twice as much Pr and Pb; 60% more U; and 20% less Sc, Tb, Dy, and Ho (**Table 2**, **Figure 3**). Most of the xenoliths in the database are mafic meta-igneous rocks, but they include ~15% metasedimentary rocks (**Figure 2**) (Hacker et al. 2011).

There are limitations to using xenoliths as samples of lower crust:

1. Xenoliths erupted from lower crustal depths may be atypical because the basaltic lavas that host most xenoliths may have insufficient buoyancy to erupt through felsic lower crust (Jaupart & Mareschal 2003) or may preferentially assimilate felsic xenoliths (Halliday et al. 1993, Rudnick & Fountain 1995).
2. Many of the xenoliths in the database do not contain garnet. This is odd for a lower crustal rock (**Supplemental Figure 1**), almost regardless of composition, and suggests that such xenoliths were not derived from lower crust (Rudnick 1992).
3. Many granulite xenoliths have Pb isotope compositions that are more evolved than those of mantle, suggesting that the xenoliths became granulites in the Phanerozoic and may not be representative of Precambrian lower crust. The Pb isotopic ratios also indicate that lower crust was once more U rich and has since been depleted in U, perhaps by Phanerozoic partial melting and melt extraction (Rudnick 1992, Rudnick & Goldstein 1990).

Supplemental Material

Because of these limitations, mafic-dominated, garnet-poor xenoliths may be unrepresentative of lower crust.

Comparison with volcanic arcs. Overall, as foreshadowed by Kelemen & Dunn (1993, figure 1) and illustrated in **Figures 3** and **4**, rock associations potentially representative of lower continental crust are strikingly similar to estimated bulk continental crust in their trace-element composition.

The compositions of granulite xenoliths and granulite- and amphibolite-facies terrains, and all previously proposed compositions for lower, upper, and bulk continental crust (**Figure 4*a*,*b***),

[1]The ability of the Al/(Ca + Na + K) metric to positively identify metasedimentary rock was assessed by testing it against true metasedimentary rocks. Post-Archean true metasedimentary rocks were scored correctly 93% of the time using Al/(Ca + Na + K), and Archean true metasedimentary rocks were scored correctly 62% of the time (**Supplemental Tables 1** and **2**). See similar analyses by Behn et al. (2011).

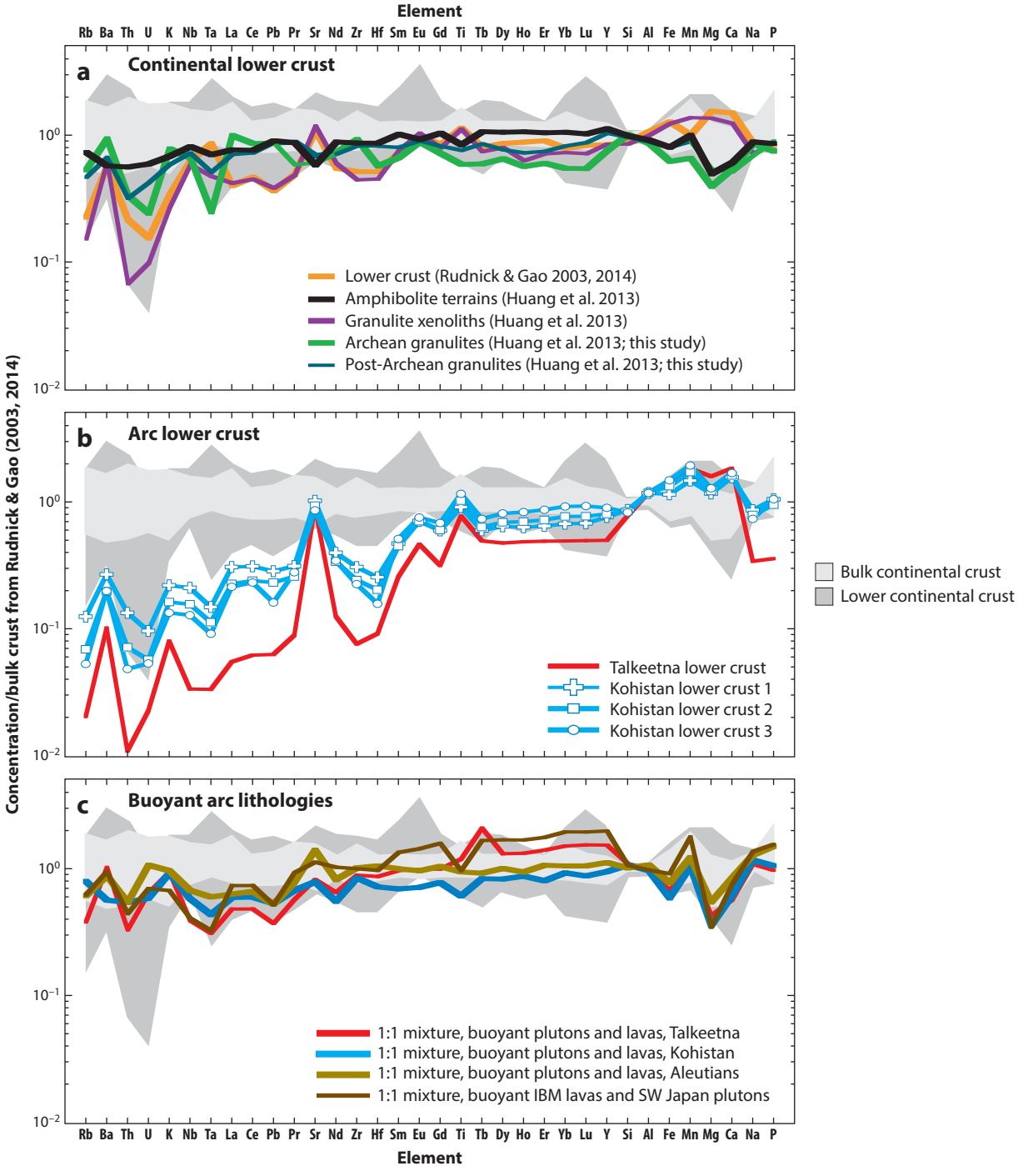

lie along a major-element trend similar to the calc-alkaline differentiation series in volcanic arcs (**Figure 4*c***)—with nearly constant Mg# [Mg/(Mg + Fe)] over a range of SiO_2 contents, as noted in many papers. We wish to emphasize once more that the calc-alkaline trend is nearly unique to volcanic arcs, whereas the tholeiitic differentiation trend—illustrated here using mid-ocean ridge basalt glasses (**Figure 4*d***)—characterizes magma from mid-ocean ridges, ocean islands, large igneous provinces, and volcanic arcs. The similarity between continental crust and calc-alkaline arc lavas and plutons, which extends to many trace-element characteristics, has given rise to the long-standing hypothesis that calc-alkaline arc magmatism—and/or geochemically similar Archean processes—played a key role in forming continental crust (e.g., Ringwood & Green 1966, Taylor 1967).

That said, it is important to note the substantial differences between the rock associations representative of continental lower crust and two well-documented examples of arc lower crust in the Jurassic Talkeetna and Cretaceous Kohistan arc sections. The lower crust compositions shown for these arcs in **Figure 3*b*** are only for gabbroic rocks that are less dense than underlying mantle peridotite; these compositions would remain in arc crust after it underwent proposed density sorting (see below). It is clear that arc lower crust is significantly depleted in MREEs, light rare earth elements (LREEs), Zr, Hf, Nb, Ta, K, U, Th, and Rb relative to any proposed continental lower crust composition, even after possible delamination has removed dense ultramafic cumulates and garnet granulites.

Heat-producing elements. Median and log-normal average values for granulite-facies metamorphic terrains and xenoliths are significantly depleted in U and Th compared with bulk continental crust, in keeping with detailed observations of Kilbourne Hole xenoliths by Reid et al. (1989). In addition, the median and log-normal average xenolith compositions are strongly depleted in Si and K relative to bulk continental crust, and strongly depleted in U and Th relative to granulite terrains and amphibolites.

Summary

The average craton, shield, and Paleozoic–Mesozoic orogen is 39–40 km thick. Cenozoic collision zones are considerably thicker, but are balanced by the 25% of continental crust that is thin and submerged, resulting in an average crustal thickness of 36 km (**Table 1**).

If the lower crust is similar to granulite-facies terrains, it may be on average dacitic to andesitic with modest radiogenic heat production. If the lower crust is similar to xenoliths, it is mafic with low radiogenic heat production. The stark difference between these choices has led to the use of heat flow and seismic wavespeeds to aid in choosing a composition for lower crust (see the next section).

Figure 3

(*a*) Log-normal average values (exp{average[ln(x_1, x_2. . .x_n)]}) of major- and trace-element concentrations from rock suites potentially representative of continental lower crust, normalized to estimated bulk continental crust from Rudnick & Gao (2003, 2014). Light and dark gray fields delineate all published estimates for bulk continental crust and lower continental crust, respectively, as compiled by Rudnick & Gao (2003, 2014) and Kelemen (1995). (*b*) Log-normal average values for the composition of arc lower crust from the Jurassic Talkeetna arc section (Kelemen et al. 2003a, 2014) and the Cretaceous Kohistan arc section (Jagoutz & Schmidt 2012), compared with selected ranges for continental lower crust. Note that the three alternative compositions for the Kohistan lower crust are log-normal average values, not average values, but use the same proportions of crustal units as did Jagoutz & Schmidt (2012). (*c*) Log-normal average values for buoyant materials from arc crust (Kelemen & Behn 2015). Abbreviation: IBM, Izu–Bonin–Mariana.

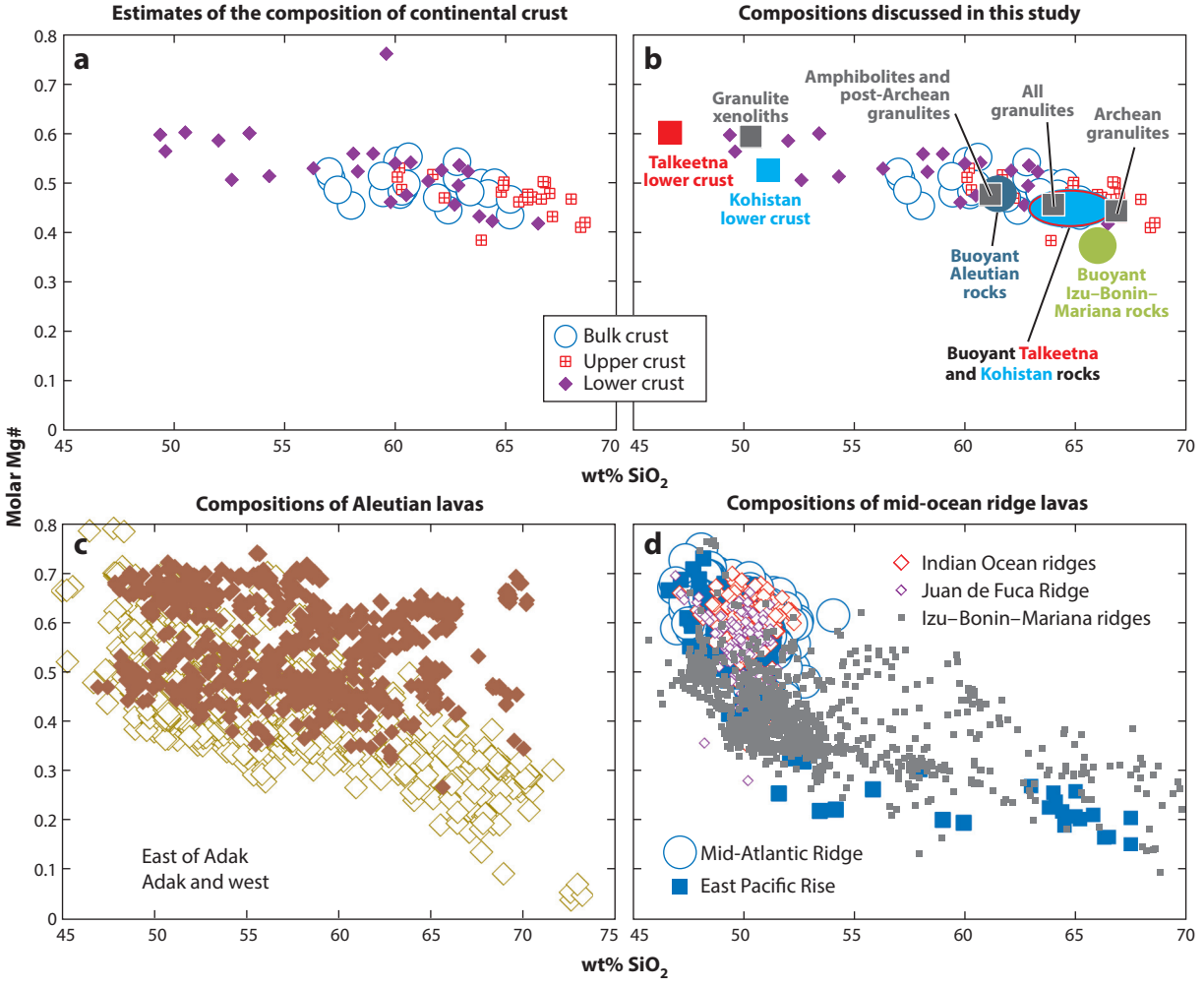

Figure 4

(*a*) Median values of wt% SiO_2 and molar Mg/(Mg + Fe), or Mg#, for published estimates of the composition of bulk, upper, and lower continental crust compiled by Rudnick & Gao (2003, 2014) and Kelemen (1995). (*b*) As for panel *a*, but with additional bulk compositions discussed in the text. Median values for buoyant arc lithologies are from Kelemen & Behn (2015). (*c*) Transitional and calc-alkaline magmatic trends as represented by Aleutian lava compositions (Kelemen et al. 2003b, Singer et al. 2007, Yogodzinski et al. 2015). (*d*) Tholeiitic magmatic trend as represented by mid-ocean ridge basalt glasses (Su 2002) and whole-rock data from mid-ocean ridges (Wanless et al. 2010) and the Izu–Bonin–Mariana arc (Jordan et al. 2012).

PHYSICAL PROPERTIES OF LOWER CONTINENTAL CRUST

Heat Production

The heat-flow balance for continental crust (surface heat flow = mantle heat flow + crustal heat production) imposes constraints on the U, Th, and K contents of lower crust (**Table 3**). Inferred abundances of heat-producing elements suggest a heat-production rate of 1.6 $\mu W/m^3$ for upper crust (Rudnick & Gao 2003, 2014). The mantle heat flow is inferred to be 11–18 mW/m^2 for Precambrian terrains and 15–21 mW/m^2 for Paleozoic orogens (Jaupart & Mareschal 2003),

Table 3 Heat production and heat flow in model crustal sections

	Heat production ($\mu W/m^3$)	Layer thickness (km)	Heat flow contribution (mW/m^2)
Most mafic model continental crust			
Upper crust	1.58	13.7	22
Middle crust	0.35	13.0	5
Lower crust	0.21	12.1	3
Mantle			17
Total surface heat flow		38.8	46
Fastest model continental crust			
Upper crust	1.58	13.7	22
Middle crust	0.34	13.0	4
Lower crust	0.17	12.1	2
Mantle			18
Total surface heat flow		38.8	46
Most felsic model continental crust			
Upper crust	1.58	13.7	22
Middle crust	0.46	13.0	6
Lower crust	0.26	12.1	3
Mantle			15
Total surface heat flow		38.8	46
Slowest model continental crust			
Upper crust	1.58	13.7	22
Middle crust	0.72	13.0	9
Lower crust	0.33	12.1	4
Mantle			11
Total surface heat flow		38.8	46
Lower model continental crust and middle continental crust are the same			
Upper crust	1.58	13.7	22
Middle crust	0.28	13.0	4
Lower crust	0.28	12.1	3
Mantle			17
Total surface heat flow		38.8	46

Thicknesses are from CRUST1.0. Surface heat flow measured in Paleozoic–Mesozoic orogens is 15–21 mW/m^2. Surface heat flow measured in shields and platforms is 11–18 mW/m^2.

though even these wide bounds are subject to the uncertainties noted by Morgan et al. (1987). Surface heat-flow measurements are quite variable (e.g., the entire range for Precambrian terrains is 15–92 mW/m^2), with averages of 46 mW/m^2 for Precambrian terrains and 58 mW/m^2 for Paleozoic terrains (Jaupart & Mareschal 2003).

In Rudnick & Gao's (2003, 2014) three-layer model, a 40-km-thick crust and a high mantle heat flow of 17 mW/m^2 require a 17-km-thick lower crust with a heat-production rate of $\leq$0.2 $\mu W/m^3$, implying that the lower crust contains a low proportion of heat-producing elements, for example, 0.6 wt% K_2O, 1.2 ppm Th, and 0.2 ppm U (**Figure 1*a***, **Supplemental Table 3*b***). This low inferred heat-production rate, together with the compositions of post-Archean continental granulite

Supplemental Material

xenoliths that were assumed to be representative of the mafic component of lower crust (see the next section), led Rudnick & Gao (2003, 2014) to the conclusion that lower crust is predominantly (80%) mafic rock. Huang et al. (2013) embraced the same concept for their 34-km-thick crustal model (**Figure 1*b***, **Supplemental Table 3*b***).

Supplemental Material

However, neither mantle heat flow nor the distribution of heat-producing elements in crust is well known. For example, if either mantle heat flow or the concentration of heat-producing elements in middle crust has been overestimated, the heat-producing element concentration in lower crust could be substantially higher, and thus the lower crust could contain more U, Th, and/or K. As an extremum (**Figure 1*c***), Hacker et al. (2011) used Michaut et al.'s (2009) lower bound on mantle heat flow through Precambrian terrains and showed that it is possible to fit the surface heat-flow constraint for a 40-km-thick crust by using a 26-km-thick lower crust with the median composition of post-Archean granulites from Rudnick & Presper (1990; database updated in 2003), with 64 wt% SiO_2 and a heat-production rate of 0.7 $\mu W/m^3$ (**Figure 1*c***). In this case, no mafic lower crust is required by the heat-flow data (**Supplemental Table 3*b***).

Wavespeeds

Seismic wavespeeds have been used to infer the composition of lower crust (Christensen & Mooney 1995, Holbrook et al. 1992, Pakiser & Robinson 1966, Rudnick & Fountain 1995) by reference to the wavespeeds of rocks measured in the laboratory (e.g., Birch 1961). Comprehensive summaries of seismic wavespeeds from lower crust were provided by Holbrook et al. (1992), Christensen & Mooney (1995), and Rudnick & Fountain (1995); additional studies are summarized in **Figure 5**. All of these studies assigned each measured crustal section to a different tectonic setting and divided the crust into layers. The median thickness of the lower crustal layer in Rudnick & Fountain's (1995) analysis is 12 $\pm$ 9 km, and that in CRUST1.0 is 11 km.

As noted in previous studies, there are clear differences in V_P of lower crust among different tectonic settings (**Figure 5**). Shields and platforms, the most abundant type at 49% area, have a relatively symmetrical distribution of speeds from 6.6–7.5 km/s. All other types of crust have a broader range of lower crust V_P, down to 6.0 km/s and up to 7.7 km/s.

The faster wavespeeds for lower crust (6.8 km/s and greater) are similar to those measured for mafic rocks in the laboratory, leading many (e.g., Christensen 1989, Christensen & Mooney 1995, Rudnick & Fountain 1995) to the conclusion that lower crust is chiefly mafic. This conclusion is not robust, however, as a large fraction of these speeds can also be satisfied by rocks that are not mafic (Behn & Kelemen 2003, Holbrook et al. 1992, Pakiser & Robinson 1966, Reid et al. 1989, Rudnick & Fountain 1995). Below we assess the utility of wavespeeds to make general inferences about the SiO_2 content of lower crust.

Using wavespeeds alone to infer crustal composition. Many papers (e.g., Kern et al. 1996, Miller & Christensen 1994, Musacchio et al. 1997, Sobolev & Babeyko 1994) have noted a relationship between rock composition and V_P, V_S, or V_P/V_S; some have implied that wavespeeds can be used to determine Earth composition at depth (see the review in Behn & Kelemen 2003). Christensen (1996), for example, reported a correlation between V_P/V_S and SiO_2 content for rocks with SiO_2 = 55–100%; the r^2 value of 0.99 reported in that paper has been taken by many to imply that V_P/V_S is an accurate predictor of the silica content of continental crust. Most recently, Huang et al. (2013) noted the correlation between SiO_2 content and laboratory V_P measurements on igneous rocks and used V_P from the CRUST2.0 model (Bassin et al. 2000) to infer the composition of lower crust. This approach has several limitations: (*i*) Lower crust is not necessarily igneous; (*ii*) the V_P values in the CRUST2.0 model are not in situ measurements but instead are

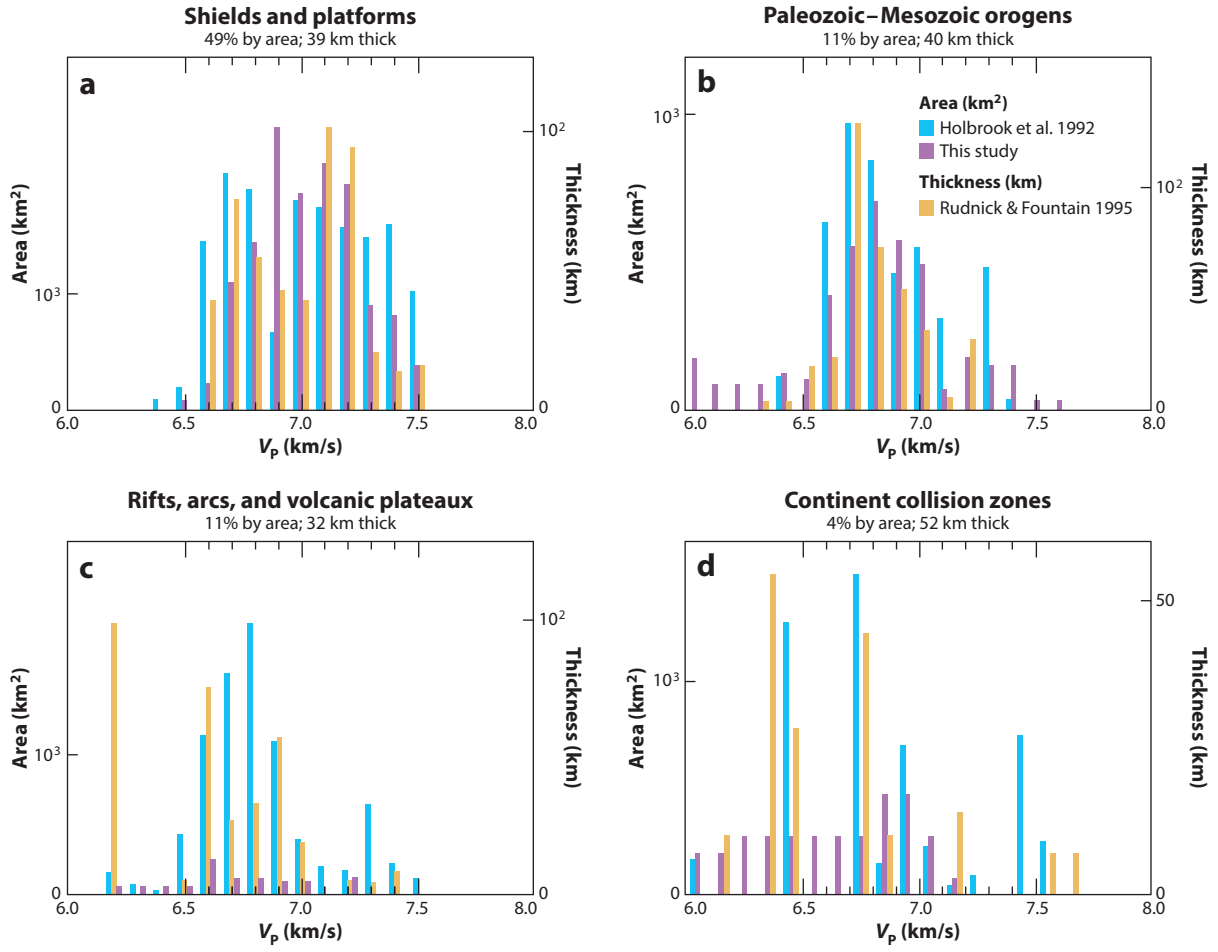

Figure 5

V_P for lower continental crust in various tectonic settings: (*a*) shields and platforms; (*b*) Paleozoic–Mesozoic orogens; (*c*) rifts, arcs, and volcanic plateaux; and (*d*) continent collision zones. The heights of bars from Holbrook et al.'s (1992) study and this study indicate cross-sectional areas of layers (references in **Supplemental Figure 4**), whereas the heights of bars from Rudnick & Fountain's (1995) study indicate thicknesses of layers. All values are as-measured, in situ lower crust speeds. Crustal thickness and areal percentage of each tectonic setting (with respect to total continental crust) are from the CRUST1.0 model; total area ≠ 100% because only some settings in CRUST1.0 are shown.

Supplemental Material

averages for different tectonic settings; (*iii*) the use of regressions yielding a single SiO_2 content for a given V_P and/or V_P/V_S obscures the fact that rocks with a variety of SiO_2 contents can have the same V_P and/or V_P/V_S; and (*iv*) the precision of measurement for V_P/V_S in middle and lower continental crust is poor.

The limitations of using wavespeeds to infer rock composition have long been appreciated (Rudnick & Fountain 1995). **Figure 6*a*,*c*,*e*** illustrates this by comparing rock wavespeeds and bulk compositions measured in the laboratory for a larger data set than was used in earlier studies. We restrict comparison to isotropic speeds and to averages of anisotropic velocities reported from laboratory experiments at 25°C and 600 MPa but include a broad range of plutonic, metasedimentary, and meta-igneous crustal rock compositions of amphibolite to granulite facies.

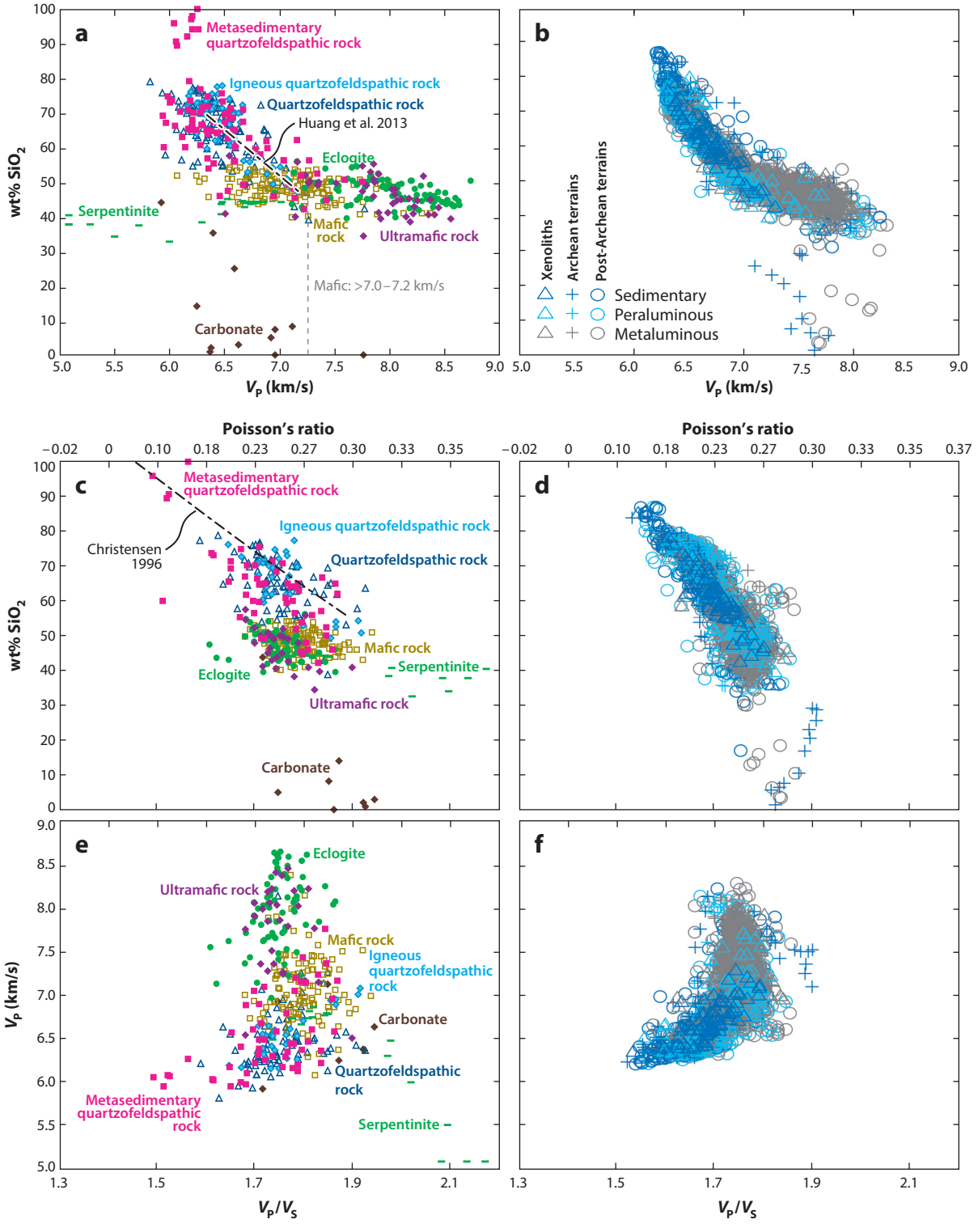

An alternative and complementary approach for estimating the relationship between seismic velocity and composition is to use a thermodynamic model to determine the mineral assemblages that crystallize from a particular bulk composition at a given pressure and temperature (**Figure 6*b*,*d*,*f***). V_P and V_S of the resulting equilibrium phase assemblage can then be estimated from the elastic properties of each constituent mineral on the basis of mixture theory (e.g., Babeyko et al. 1994, Sobolev & Babeyko 1994). This approach avoids some of the difficulties associated with laboratory measurements by eliminating the problem of residual porosity or alteration and allowing efficient calculation of seismic velocities for many compositions over a wide range of *P-T* conditions (e.g., Behn & Kelemen 2003, 2006), but it is limited by the accuracy of the thermodynamic models and elastic moduli. **Figure 6*b*,*d*,*f*** shows seismic velocities calculated from the thermodynamic software Perple_X for Huang et al.'s (2013) database of xenolith compositions and our updated compilation of samples from Archean and post-Archean terrains (**Tables 1** and **2**). These calculations yield remarkably similar relationships between V_P and V_P/V_S compared with the laboratory data.

Figure 6 shows that, regardless of approach, there are limits to the accuracy with which composition can be inferred from isotropic V_P and/or V_P/V_S. The reason for this is that the wavespeeds of quite different rocks overlap substantially. For example, rocks ranging in composition from quartzose (80% SiO_2) to carbonate (0% SiO_2) to mafic all can have V_P = 6.5–7.2 km/s and V_P/V_S = 1.6–1.9. Because experimentalists have focused on mafic lithologies, commonly inferred to comprise both continental and oceanic lower crust, a histogram of SiO_2 content for experimental samples with, for example, V_P/V_S from 1.71 to 1.76 indicates that a majority of these samples have SiO_2 < 55 wt% (**Supplemental Figure 2**). However, in contrast, a histogram of V_P/V_S for samples with 55 to 65 wt% SiO_2 indicates that the most common V_P/V_S for such samples is also between 1.71 and 1.76.

Supplemental Material

In addition to the various uncertainties in linking SiO_2 to seismic wavespeeds, SiO_2 is not well correlated with rock composition. A material with 50–60 wt% SiO_2 could be mafic (e.g., a gabbro), but it could also be aluminous metasedimentary rock or quartzofeldspathic rock of sedimentary or igneous provenance. Thus, statements such as "With the exception of marble and anorthosite, rocks with velocities between 6.5 km/s and 7. 0 km/s are mafic" (Christensen & Mooney 1995, p. 9779) are misleading. However, wavespeeds greater than 7.0–7.2 km/s, depending on the geotherm, are reasonably reliable indicators of mafic lower crust (<55 wt% SiO_2); this limit is marked by the dotted line labeled "mafic" in **Figure 6*a***.

Extrapolating laboratory V_P and V_P/V_S to lower crustal conditions. To be able to interpret lower crustal wavespeeds, data measured at laboratory conditions (e.g., 25°C and 0.6 GPa) must be extrapolated to lower crustal conditions. This extrapolation is usually done using scalars for $\partial V/\partial T$ and $\partial V/\partial P$ (e.g., Christensen 1989, Rudnick & Fountain 1995). The accuracy of this approach can be seen in **Supplemental Figure 3**, which depicts the correction that must be applied to extrapolate V_P and V_P/V_S measured at 25°C and 0.6 GPa to ambient lower crustal conditions of 1 GPa and 300°C, 500°C, and 900°C [conditions that correspond to the "cold," "average," and "hot" orogens of Christensen & Mooney (1995). It is clear from **Figure 6** that linear relationships

Figure 6

Wavespeed versus SiO_2 at 25°C and 600 MPa, measured for a broad range of rocks (panels *a*, *c*, and *e*; references in **Supplemental Figure 2**) and calculated for granulite-facies xenoliths and terrains (panels *b*, *d*, and *f*). V_P and V_P/V_S are generally poor indicators of SiO_2 content and even poorer indicators of rock type. The dashed line in panel *a* shows the approximate limit on the velocities of mafic rock in crust with cold and average thermal gradients (see **Figure 7**).

do not fit all rock types or *P-T* conditions: extrapolation is modest for "cold" and "average" orogens (e.g., ~0.15 km/s for V_P) but large for SiO_2-rich compositions in "hot" orogens because of the odd elastic properties of quartz. We improve on the linear $\partial V/\partial T$ and $\partial V/\partial P$ approach by correcting laboratory measurements in **Figure 6** using the relationships in **Supplemental Figure 3** and applying it to the data sets in **Figure 5**. This results in minor displacements of the "mafic" discriminant boundary in **Figure 7*a*,*b*** relative to **Figure 6**, and more significant shifts in **Figure 7*c*,*d***.

Mafic rock in lower crust. The locations of the "mafic" discriminant boundaries in **Figures 6** and **7** indicate that most lower crustal V_P measurements are not indicative of a specific rock type and could correspond to mafic or felsic rock. Only a fraction of the reported V_P values require the presence of mafic rocks in lower crust. To quantify the amount of mafic lower crust that must be present in various tectonic settings, we compute the fraction of V_P values faster than the "mafic" discriminant boundaries in **Figures 6** and **7** (indicated with gray brackets in **Figure 7**). We use three methods: (*i*) the cross-sectional areas of Holbrook et al.'s (1992) measurements, (*ii*) the cross-sectional areas of the additional data in **Figure 5**, and (*iii*) the layer thicknesses in Rudnick & Fountain's (1995) data; we do not use the thickness of the lower crust nodes in CRUST1.0 because these are averages that obscure fast outliers. These percentages are subject to considerable uncertainty, but they indicate that ~20–30% of the lower crust beneath shields (corresponding to a thickness of ~2.2–3.3 km) must be mafic and ~10–20% of the lower crust elsewhere (~1.2–2.4 km) must also be mafic. Weighting these percentages by the area of the four tectonic settings in **Figure 7** suggests that ~20% (2.4 km) of the overall lower crust must be mafic.

MOST LOWER CRUST NEED NOT BE MAFIC

Thus, seismic wavespeeds constrain the composition of a restricted portion of lower crust but do not constrain the composition of most lower crust. Lower crust could be relatively felsic, like granulite- and amphibolite-facies terrains, or relatively mafic, like continental granulite xenoliths. These points are quantitatively illustrated in **Figures 8** and **9**. Both figures use the compositions of granulite-facies terrains, granulite-facies xenoliths, and amphibolite-facies terrains in **Supplemental Tables 1** and **2** and from Huang et al. (2013). The seismic properties and densities were calculated using Perple_X (version 6.6.7) for these compositions, assuming 1 wt% H_2O (amphibolites) or 0.5 wt% H_2O (granulites). For lower crust, wavespeeds and densities were calculated at 500°C and 1.0 GPa for phase assemblages equilibrated at 650°C (amphibolites) or 750°C (granulites) and 1.0 GPa. For middle crust, wavespeeds and densities were calculated at 375°C and 0.7 GPa for phase assemblages equilibrated at 650°C (amphibolites) or 700°C (granulites) and 0.7 GPa.

We compare these thermodynamic calculations to our global compilation of seismic wavespeeds for the lower and middle continental crust (**Supplemental Figure 4**). Lower crust is dominated by $V_P = 6.7–7.3$ km/s and $V_P/V_S = 1.67–1.78$; broader V_P/V_S bounds of 1.68–1.85 are indicated by Poisson's ratios of 0.25–0.27 and 2% uncertainties in V_P and V_S. As illustrated in **Supplemental Figure 4**, middle crust is dominated by $V_P = 6.5–6.8$ km/s and $V_P/V_S = 1.65–1.80$.

Figure 9 summarizes the compositions of samples that could comprise middle and lower continental crust based on seismic wavespeeds. From these data, middle crust could have between 49 and 88 wt% SiO_2 (90% of the samples have a narrower bound, 54–78 wt% SiO_2), and lower crust could have between 40 and 66 wt% SiO_2 (90% have 48–61 wt% SiO_2). There is a broad compositional range of samples, with 49 to 66 wt% SiO_2, that could be representative of both middle and lower crust (red circles in **Figure 9**). Thus, there is no requirement from seismic

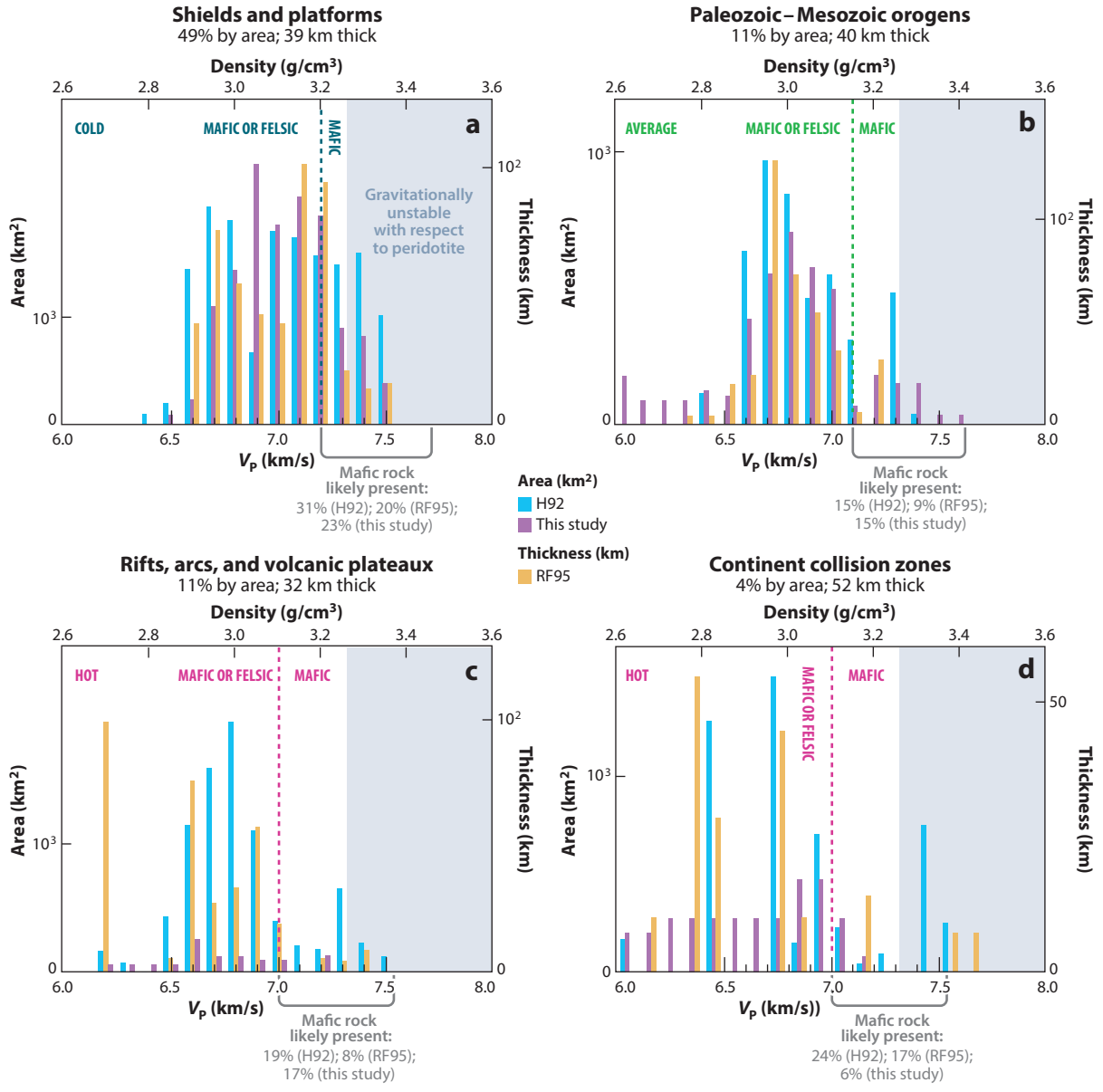

Figure 7

Use of V_P to assess mafic rock content and density instability of lower crust: (*a*) shields and platforms; (*b*) Paleozoic–Mesozoic orogens; (*c*) rifts, arcs, and volcanic plateaux; and (*d*) continent collision zones. Mafic rocks are likely present at V_P above the discriminant dotted line (from **Figure 6**, adjusted for "cold," "average," and "hot" geotherms). Gray brackets show the percentage of mafic rocks by area from H92 (Holbrook et al. 1992) and this study, and by thickness from RF95 (Rudnick & Fountain 1995). The majority of V_P measurements from lower crust (**Figure 5**) are not indicative of a specific rock type and could be from quartzofeldspathic rock, mafic rock, or a mixture thereof; mafic rocks comprise significant sections of the lower crust of shields and platforms and of rifts, arcs, volcanic plateaux. Densities of lower crust are inferred from V_P (**Supplemental Figure 5**). Densities likely to be gravitationally unstable with respect to the underlying mantle fall in gray fields. Most lower continental crust is gravitationally stable.

Supplemental Material

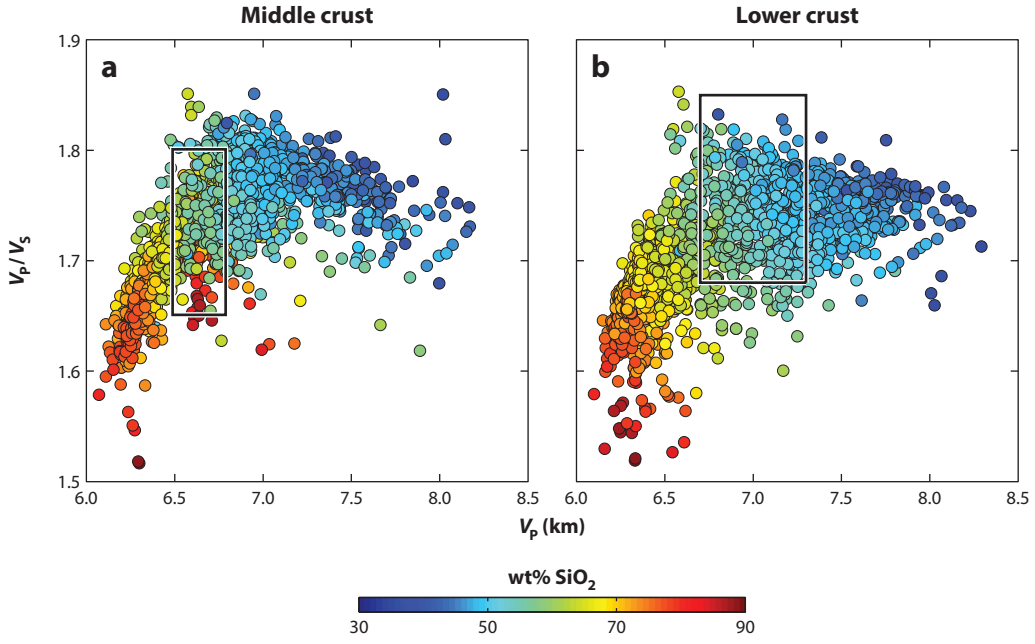

Figure 8

Calculated V_P and V_P/V_S for samples of amphibolite- and granulite-facies terrains and xenoliths. Boxes indicate bounds for continental crust beneath shields and platforms and Paleozoic–Mesozoic orogens (see text and **Supplemental Figure 4**): (*a*) Middle crust V_P = 6.5–6.8 km/s and V_P/V_S = 1.65–1.80, and (*b*) lower crust V_P = 6.7–7.3 km/s and V_P/V_S = 1.68–1.85.

Supplemental Material

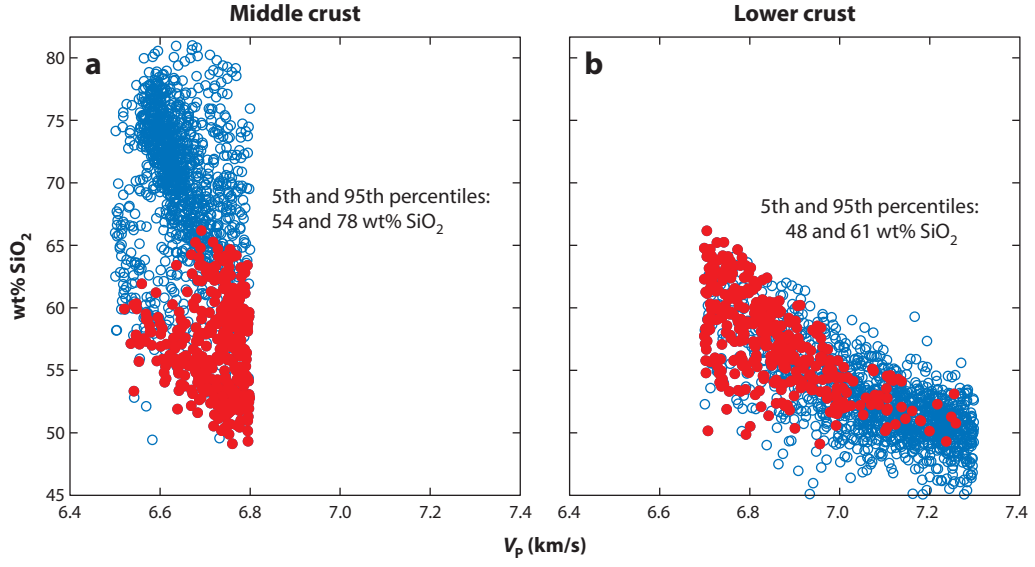

Figure 9

Relationships between SiO_2 and V_P of amphibolite- to granulite-facies xenolith and terrain samples with calculated V_P and V_P/V_S values that match observed constraints for (*a*) middle crust or (*b*) lower crust of shields and platforms and Paleozoic–Mesozoic orogens. Red circles indicate rocks that satisfy constraints for both middle and lower crust.

wavespeeds for systematic SiO_2 variation as a function of depth in the middle and lower continental crust. Instead, gradually increasing V_P with depth could be due to mineralogical changes in rocks of constant average SiO_2 content.

Unlike the compiled data for all granulite-facies samples, there is a broad correlation between V_P and SiO_2 among the samples that fit the lower crustal seismic constraints (**Figure 9**). No such relationship is observed for samples that fit middle crustal seismic constraints. We stress that the sample compositions that are consistent with seismic constraints are not distributions with a significant mean value and variation due to measurement uncertainty—they are simply ranges of permissible values. Thus, there is no reason to infer that a sample in the center of these ranges is any more or less likely to be representative of middle or lower crust than is a sample near the outer bounds.

To emphasize the point that a range of major-element and median trace-element compositions are consistent with the seismic constraints, **Table 4** shows two endmembers that span the range of SiO_2 values and two endmembers that span the range of V_P values in **Figure 9**. The compositions are compared with other estimates of bulk continental crust and lower crust in **Figure 10**. **Supplemental Table 4** provides additional data for compositions that lie between these endmembers.

Supplemental Material

Potential Lower and Middle Continental Crust Compositions

In **Figure 11**, **Table 3**, and **Supplemental Table 3**, we explore the additional constraints that heat flow provides on the composition of lower crust. We focus on shields and platforms because they have the best-measured heat flow, their geotherms are more likely to be in steady state, and they constitute half of Earth's continental crust (**Table 1**).

Table 4 summarizes average compositions derived from the calculations illustrated in **Figures 8** and **9**, with calculated heat production for a variety of possible middle and lower crustal compositions and calculated heat flow for bulk crust formed from various possible combinations of upper, middle, and lower crust compositions. We provide averages for samples satisfying lower crustal constraints that have 45–50 wt% SiO_2 (average $V_P = 7.2$), $V_P = 7.1$–7.3 km/s (average 51 wt% SiO_2), 60–65 wt% SiO_2 (average $V_P = 6.8$), and $V_P = 6.7$–6.9 km/s (average 58 wt% SiO_2). Similarly, we provide averages within selected bounds of SiO_2 and V_P for samples meeting middle crustal constraints. These have 53, 63, 68, and 70 wt% SiO_2 and $V_P = 6.7$, 6.7, 6.7, and 6.6 km/s, respectively. We also provide average compositions for the case in which middle and lower crust have the same composition, with 57 wt% SiO_2. This composition has lower and middle crustal V_P of 6.9 and 6.7 km/s, respectively. All these different potential lower and middle crust compositions have V_P/V_S ratios of 1.71–1.76, within the range of observed values (**Supplemental Figure 4**).

Combining the most-mafic middle and lower crust averages yields a bulk crust with 56 wt% SiO_2. For shields and platforms with a mantle heat flow of 11–18 mW/m^2, this combination leads to a surface heat flow of 40–47 mW/m^2 (**Tables 3** and **4**, **Supplemental Table 3**). Combining the most-felsic middle and lower crust averages gives a bulk crust with 65 wt% SiO_2 and a surface heat flow of 42–49 mW/m^2. Crust made of the fastest-V_P compositions yields 60 wt% SiO_2 and heat flow of 39–46 mW/m^2, and a combination of the slowest-V_P compositions gives a bulk crust with 65 wt% SiO_2 and heat flow of 46–53 mW/m^2. For the case in which the middle and lower crust are the same, the bulk crust has 60 wt% SiO_2 and a surface heat flow of 40–47 mW/m^2.

A number of assumptions and poorly known parameters are included in these calculations, but they serve to emphasize that heat flow alone provides minimal constraints on the composition of lower crust. All of the calculated values match the observed average of 46 mW/m^2 (**Figure 11**) (Jaupart & Mareschal 2003). Further, these calculations suggest that, in some places,

Table 4 Endmember, bulk continental crust, and lower crust compositions that satisfy V_P, V_P/V_S, and heat-flow constraints

Erratum

	Endmember lower crust compositions				Endmember middle crust compositions				Lower, middle crust the same	
	Lower crust 45–50 wt% SiO_2	Lower crust V_P 7.1–7.3 km/s	Lower crust 60–65 wt% SiO_2	Lower crust V_P 6.7–6.9 km/s	Middle crust 50–55 wt% SiO_2	Middle crust V_P 6.7–6.8 km/s	Middle crust 65–70 wt% SiO_2	Middle crust V_P 6.5–6.6 km/s	Lower	Middle
% of all granulite and amphibolite samples	6	15	3	10	3	12	7	7	8	8
% of samples that fit seismic constraints	17	42	8	27	8	33	20	21	23	23
V_P (km/s), *avg*	7.18	7.20	6.77	6.80	6.73	6.75	6.67	6.57	6.86	6.72
V_S (km/s), *avg*	4.07	4.13	3.95	3.92	3.83	3.86	3.83	3.80	3.96	3.82
V_P/V_S, *avg*	1.76	1.74	1.71	1.74	1.76	1.75	1.74	1.73	1.73	1.76
Density (kg/m^3), *avg*	3,187	3,194	2,921	2,964	2,992	2,850	2,750	2,720	3,006	2,905
Heat production (μW/m^3), ln(*avg*)	0.21	0.17	0.26	0.33	0.35	0.34	0.46	0.72	0.28	0.28
SiO_2 (wt%), *avg*	48.6	50.7	61.9	58.0	53.1	62.7	67.7	69.9	57.3	57.3
TiO_2 (wt%), *avg*	1.40	1.24	0.78	0.91	1.26	0.80	0.55	0.41	0.99	0.99
Al_2O_3 (wt%), *avg*	18.1	16.5	16.1	17.5	16.7	15.7	15.6	14.9	16.8	16.8
FeO^T (wt%), *avg*	10.44	10.39	6.52	7.41	10.32	6.76	4.46	3.55	8.15	8.15
MnO (wt%), *avg*	0.18	0.19	0.11	0.13	0.21	0.13	0.08	0.07	0.16	0.16
MgO (wt%), *avg*	6.87	7.03	3.14	3.93	5.98	3.51	1.72	1.29	4.46	4.46
CaO (wt%), *avg*	10.11	10.10	5.77	6.23	7.48	5.27	3.62	2.50	6.63	6.63
Na_2O (wt%), *avg*	2.85	2.80	3.92	3.82	3.38	3.42	3.88	3.85	3.89	3.89
K_2O (wt%), *avg*	1.22	0.79	1.54	1.86	1.29	1.60	2.26	3.42	1.42	1.42
P_2O_5 (wt%), *avg*	0.23	0.22	0.21	0.25	0.24	0.20	0.18	0.12	0.24	0.24
Mg#	54	55	46	49	51	48	41	39	49	49
Rb (ppm), *ln-avg*	17	10	14	24	19	21	22	63	18	18
Ba (ppm), *ln-avg*	204	168	419	468	173	373	554	524	310	310
Th (ppm), *ln-avg*	0.75	0.59	1.26	1.19	1.88	1.77	0.57	4.06	1.19	1.19
U (ppm), *ln-avg*	0.25	0.20	0.29	0.34	0.49	0.44	0.21	0.92	0.37	0.37
K (ppm), *ln-avg*	6,434	4,659	9,292	11,617	6,632	9,464	12,303	21,283	8,508	8,508
Nb (ppm), *ln-avg*	4.9	4.3	7.1	7.3	5.6	6.1	4.9	7.0	6.2	6.2
Ta (ppm), *ln-avg*	0.34	0.28	0.42	0.39	0.40	0.40	0.23	0.35	0.34	0.34
La (ppm), *ln-avg*	8	8	20	19	13	18	18	22	16	16
Ce (ppm), *ln-avg*	19	18	46	41	27	37	39	47	34	34
Pb (ppm), *ln-avg*	5.3	5.0	10.2	9.8	6.6	10.2	7.7	15.7	9.1	9.1
Pr (ppm), *ln-avg*	2.5	2.3	5.1	5.0	4.2	4.5	4.1	5.4	4.5	4.5
Sr (ppm), *ln-avg*	289	270	320	390	221	288	517	184	320	320
Nd (ppm), *ln-avg*	13	12	22	22	16	19	19	20	19	19
Zr (ppm), *ln-avg*	72	72	127	125	98	121	122	136	111	111
Hf (ppm), *ln-avg*	1.7	1.8	3.5	3.1	2.3	3.1	3.1	3.7	2.5	2.5
Sm (ppm), *ln-avg*	2.9	3.1	4.1	4.2	4.1	3.8	3.5	3.2	4.1	4.1
Eu (ppm), *ln-avg*	1.1	1.2	1.1	1.4	1.3	1.2	1.3	1.0	1.3	1.3
Gd (ppm), *ln-avg*	3.5	3.4	3.7	3.6	3.9	3.5	3.1	3.4	3.7	3.7
Ti (ppm), *ln-avg*	6,318	6,194	4,412	4,714	6,753	4,152	3,559	1,515	5,297	5,297
Tb (ppm), *ln-avg*	0.52	0.59	0.66	0.60	0.77	0.61	0.42	0.40	0.67	0.67
Dy (ppm), *ln-avg*	3.6	3.7	3.1	3.1	4.3	3.3	2.0	2.9	3.7	3.7
Ho (ppm), *ln-avg*	0.75	0.77	0.61	0.63	0.94	0.68	0.39	0.58	0.76	0.76
Er (ppm), *ln-avg*	2.0	2.1	1.6	1.6	2.5	1.8	1.2	1.6	2.0	2.0
Yb (ppm), *ln-avg*	1.8	2.0	1.5	1.4	2.3	1.7	1.1	1.2	1.7	1.7
Lu (ppm), *ln-avg*	0.30	0.31	0.24	0.25	0.38	0.28	0.16	0.20	0.29	0.29
Y (ppm), *ln-avg*	21	22	20.6	19.7	23.9	19.8	11.0	19.1	21.2	21.2

Table 4 (*Continued*)

Upper crust 13.7 km Middle crust 13.0 km Lower crust 12.1 km Upper crust density 2,700 kg/m³ Heat production 1.58 μW/m³ Mantle heat flow 11–18 mW/m²	Calculated bulk crust compositions					Rudnick & Gao (2003, 2014)			
	Most-mafic middle and lower crust	Fastest-V_p middle and lower crust	Most-felsic middle and lower crust	Slowest-V_p middle and lower crust	Lower, middle crust the same	Upper crust	Middle crust	Lower crust	Bulk crust
Upper crust (wt%)	32	33	34	34	33				
Middle crust (wt%)	34	33	33	33	34				
Lower crust (wt%)	34	34	33	33	33				
Crustal density (kg/m³)	2,950	2,904	2,786	2,789	2,864				
Surface heat flow (mW/m²)	40–47	39–46	42–49	46–53	40–47				
SiO_2 (wt%)	56.0	59.9	65.4	64.8	60.4	66.6	63.5	53.4	60.6
TiO_2 (wt%)	1.11	0.90	0.66	0.65	0.88	0.64	0.69	0.82	0.72
Al_2O_3 (wt%)	16.7	15.9	15.7	15.9	16.3	15.4	15.0	16.9	15.9
FeO^T (wt%)	8.65	7.44	5.33	5.34	7.12	5.04	6.02	8.57	6.71
MnO (wt%)	0.17	0.14	0.10	0.10	0.14	0.10	0.10	0.10	0.10
MgO (wt%)	5.15	4.38	2.44	2.57	3.80	2.48	3.59	7.24	4.66
CaO (wt%)	7.11	6.38	4.31	4.11	5.62	3.59	5.25	9.59	6.41
Na_2O (wt%)	3.17	3.16	3.68	3.64	3.69	3.27	3.39	2.65	3.07
K_2O (wt%)	1.75	1.71	2.21	2.69	1.88	2.80	2.30	0.61	1.81
P_2O_5 (wt%)	0.21	0.19	0.18	0.17	0.21	0.15	0.15	0.10	0.13
Mg#	51	51	45	46	49	47	52	60	55
Rb (ppm)	39	38	41	58	40	84	65	11	49
Ba (ppm)	329	385	534	540	415	624	532	259	456
Th (ppm)	4.29	4.23	4.20	5.31	4.29	10.5	6.5	1.2	5.6
U (ppm)	1.13	1.10	1.09	1.33	1.14	2.70	1.30	0.20	1.30
K (ppm)	11,934	12,340	15,063	18,750	13,413	23,244	19,093	5,064	15,025
Nb (ppm)	7.4	7.4	8.1	8.8	8.1	12.0	10.0	5.0	8.0
Ta (ppm)	0.54	0.52	0.52	0.55	0.53	0.90	0.60	0.60	0.70
La (ppm)	17	19	23	24	21	31	24	8	20
Ce (ppm)	36	39	49	51	44	63	53	20	43
Pb (ppm)	9.5	10.7	11.7	14.2	11.7	17.0	15.2	4.0	11.0
Pr (ppm)	4.5	4.6	5.5	5.8	5.3	7.1	5.8	2.4	4.9
Sr (ppm)	276	292	385	299	320	320	282	348	320
Nd (ppm)	19	19	23	23	22	27	25	11	20
Zr (ppm)	120	128	148	152	138	193	149	68	132
Hf (ppm)	3.1	3.4	4.0	4.0	3.4	5.3	4.4	1.9	3.7
Sm (ppm)	3.9	3.9	4.1	4.0	4.3	4.7	4.6	2.8	3.9
Eu (ppm)	1.1	1.1	1.1	1.1	1.2	1.0	1.4	1.1	1.1
Gd (ppm)	3.8	3.6	3.6	3.7	3.8	4.0	4.0	3.1	3.7
Ti (ppm)	5,663	4,749	3,932	3,369	4,810	3,836	4,136	4,915	4,315
Tb (ppm)	0.66	0.63	0.59	0.57	0.68	0.70	0.70	0.48	0.60
Dy (ppm)	3.9	3.6	3.0	3.3	3.7	3.9	3.8	3.1	3.6
Ho (ppm)	0.84	0.76	0.61	0.68	0.79	0.83	0.82	0.68	0.77
Er (ppm)	2.3	2.1	1.7	1.9	2.1	2.3	2.3	1.9	2.1
Yb (ppm)	2.1	1.9	1.6	1.6	1.8	2.0	2.2	1.5	1.9
Lu (ppm)	0.33	0.30	0.24	0.25	0.30	0.31	0.40	0.25	0.30
Y (ppm)	22	21	18	20	21	21	20	16	19

Table 4 (*Continued*)

	Endmember lower crust compositions divided by Rudnick & Gao: lower crust				Endmember middle crust compositions divided by Rudnick & Gao: middle crust				Divided by RG lower	Divided by RG middle
	Lower crust 45–50 wt% SiO_2	Lower crust V_P 7.1–7.3 km/s	Lower crust 60–65 wt% SiO_2	Lower crust V_P 6.7–6.9 km/s	Middle crust 50–55 wt% SiO_2	Middle crust V_P 6.7–6.8 km/s	Middle crust 65–70 wt% SiO_2	Middle crust V_P 6.5–6.6 km/s	Lower, middle crust the same	Lower, middle crust the same
Si	0.91	0.95	1.16	1.09	0.84	0.99	1.07	1.10	1.07	0.90
Ti	1.70	1.51	0.95	1.10	1.83	1.16	0.80	0.60	1.21	1.44
Al	1.07	0.98	0.95	1.03	1.11	1.04	1.04	0.99	0.99	1.12
Fe	1.22	1.21	0.76	0.86	1.71	1.12	0.74	0.59	0.95	1.35
Mn	1.80	1.90	1.13	1.31	2.13	1.26	0.81	0.68	1.56	1.56
Mg	0.95	0.97	0.43	0.54	1.67	0.98	0.48	0.36	0.62	1.24
Ca	1.05	1.05	0.60	0.65	1.43	1.00	0.69	0.48	0.69	1.26
Na	1.08	1.06	1.48	1.44	1.00	1.01	1.14	1.14	1.47	1.15
K	2.00	1.29	2.52	3.05	0.56	0.69	0.98	1.49	2.33	0.62
P	2.33	2.24	2.07	2.50	1.63	1.30	1.23	0.78	2.41	1.60
Rb	1.54	0.89	1.32	2.22	0.29	0.32	0.34	0.98	1.63	0.28
Ba	0.79	0.65	1.62	1.81	0.33	0.70	1.04	0.99	1.20	0.58
Th	0.63	0.49	1.05	0.99	0.29	0.27	0.09	0.63	0.99	0.18
U	1.26	1.02	1.43	1.69	0.38	0.34	0.16	0.70	1.84	0.28
K	1.27	0.92	1.83	2.29	0.35	0.50	0.64	1.11	1.68	0.45
Nb	0.97	0.85	1.42	1.45	0.56	0.61	0.49	0.70	1.23	0.62
Ta	0.57	0.46	0.71	0.65	0.67	0.66	0.38	0.58	0.57	0.57
La	1.02	0.96	2.46	2.39	0.52	0.74	0.74	0.91	1.98	0.66
Ce	0.96	0.91	2.30	2.07	0.50	0.71	0.73	0.89	1.70	0.64
Pb	1.33	1.25	2.55	2.45	0.44	0.67	0.51	1.03	2.28	0.60
Pr	1.04	0.97	2.14	2.07	0.72	0.78	0.71	0.93	1.86	0.77
Sr	0.83	0.78	0.92	1.12	0.78	1.02	1.83	0.65	0.92	1.13
Nd	1.16	1.05	2.00	1.97	0.65	0.74	0.75	0.82	1.73	0.76
Zr	1.06	1.06	1.87	1.84	0.66	0.81	0.82	0.91	1.63	0.74
Hf	0.91	0.95	1.86	1.63	0.52	0.70	0.71	0.83	1.31	0.57
Sm	1.05	1.10	1.46	1.49	0.88	0.83	0.76	0.69	1.46	0.89
Eu	1.01	1.10	1.02	1.26	0.92	0.84	0.90	0.69	1.15	0.90
Gd	1.14	1.10	1.19	1.18	0.96	0.87	0.76	0.84	1.19	0.93
Ti	1.29	1.26	0.90	0.96	1.63	1.00	0.86	0.37	1.08	1.28
Tb	1.08	1.22	1.37	1.24	1.10	0.87	0.59	0.58	1.39	0.95
Dy	1.16	1.18	1.01	1.00	1.13	0.87	0.52	0.76	1.18	0.96
Ho	1.10	1.13	0.89	0.93	1.15	0.83	0.48	0.70	1.12	0.93
Er	1.07	1.13	0.87	0.87	1.08	0.80	0.51	0.71	1.06	0.88
Yb	1.23	1.31	0.99	0.96	1.06	0.75	0.52	0.56	1.16	0.79
Lu	1.18	1.23	0.96	1.00	0.94	0.71	0.41	0.50	1.16	0.73
Y	1.33	1.36	1.28	1.23	1.20	0.99	0.55	0.95	1.32	1.06

Major element values in red are more than 5% lower than Rudnick & Gao (2003, 2014)

Trace element values in red are more than 5% lower than Rudnick & Gao (2003, 2014)

Major element values in blue are more than 5% higher than Rudnick & Gao (2003, 2014)

Trace element values in blue are more than 10% higher than Rudnick & Gao (2003, 2014)

Table 4 (*Continued*)

	Calculated bulk crust compositions divided by Rudnick & Gao middle crust				
	Most-mafic middle and lower crust	Highest-V_P middle and lower crust	Most-felsic middle and lower crust	Lowest-V_P middle and lower crust	Lower, middle crust the same
Si	0.92	0.99	1.08	1.07	1.00
Ti	1.54	1.25	0.91	0.91	1.22
Al	1.05	1.00	0.99	1.00	1.03
Fe	1.29	1.11	0.79	0.80	1.06
Mn	1.65	1.39	0.98	1.00	1.37
Mg	1.11	0.94	0.52	0.55	0.82
Ca	1.11	0.99	0.67	0.64	0.88
Na	1.03	1.03	1.20	1.19	1.20
K	0.97	0.95	1.22	1.49	1.04
P	1.61	1.46	1.38	1.33	1.62
Rb	0.80	0.77	0.83	1.17	0.81
Ba	0.72	0.84	1.17	1.18	0.91
Th	0.77	0.76	0.75	0.95	0.77
U	0.87	0.85	0.83	1.03	0.88
K	0.79	0.82	1.00	1.25	0.89
Nb	0.93	0.92	1.01	1.10	1.01
Ta	0.77	0.74	0.74	0.78	0.75
La	0.85	0.93	1.14	1.20	1.05
Ce	0.84	0.91	1.15	1.18	1.02
Pb	0.87	0.97	1.06	1.29	1.07
Pr	0.93	0.94	1.12	1.19	1.09
Sr	0.86	0.91	1.20	0.93	1.00
Nd	0.93	0.95	1.13	1.15	1.09
Zr	0.91	0.97	1.12	1.15	1.05
Hf	0.83	0.91	1.08	1.09	0.93
Sm	1.00	0.99	1.05	1.03	1.10
Eu	1.03	1.03	1.02	1.02	1.07
Gd	1.03	0.98	0.97	0.99	1.03
Ti	1.31	1.10	0.91	0.78	1.11
Tb	1.11	1.05	0.99	0.95	1.13
Dy	1.09	1.01	0.84	0.92	1.04
Ho	1.09	0.99	0.79	0.88	1.02
Er	1.08	1.00	0.82	0.89	1.00
Yb	1.09	0.99	0.82	0.82	0.96
Lu	1.09	1.00	0.80	0.85	0.99
Y	1.16	1.10	0.92	1.05	1.11

Major element values in red are more than 5% lower than Rudnick & Gao (2003, 2014)

Trace element values in red are more than 5% lower than Rudnick & Gao (2003, 2014)

Major element values in blue are more than 5% higher than Rudnick & Gao (2003, 2014)

Trace element values in blue are more than 10% higher than Rudnick & Gao (2003, 2014)

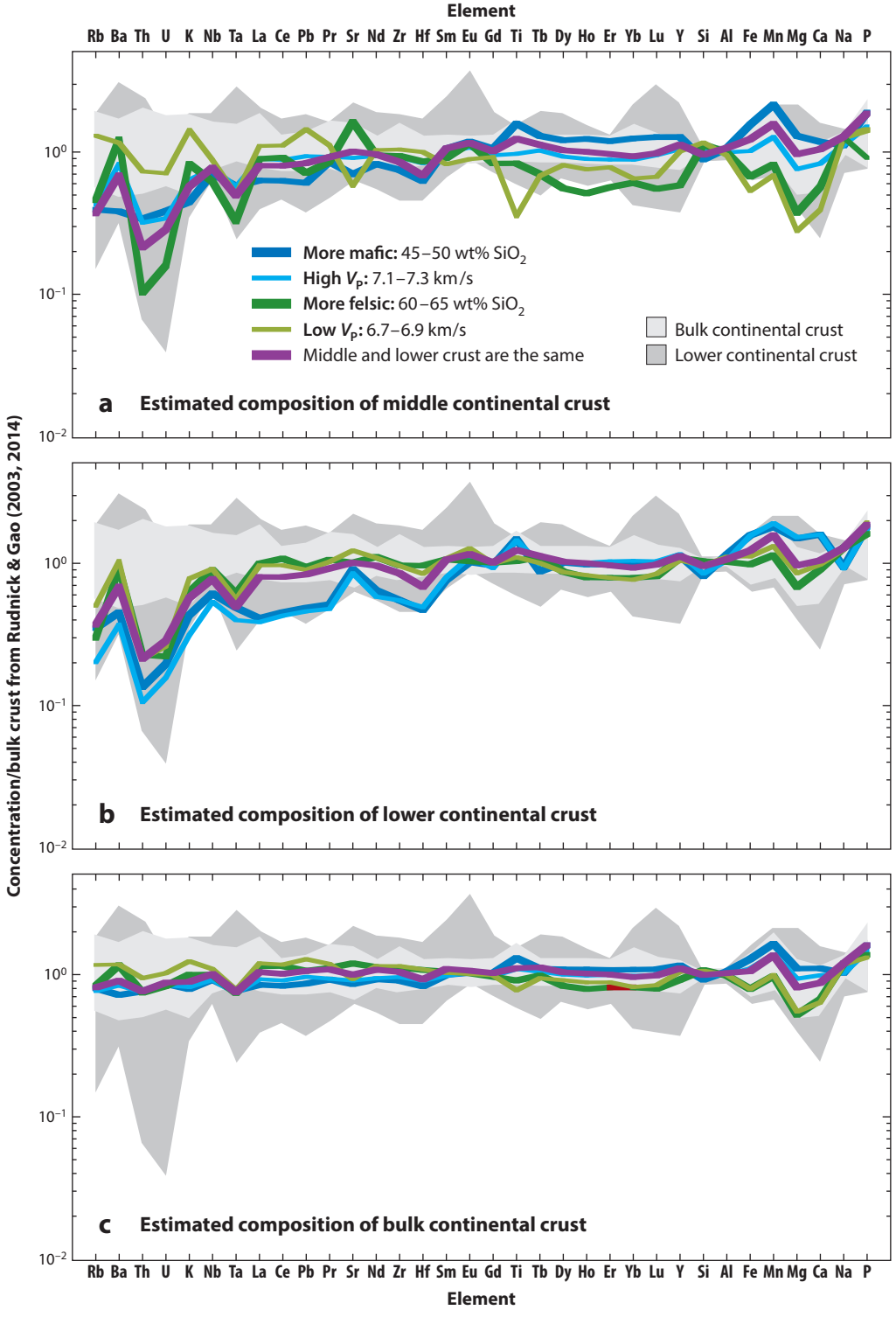

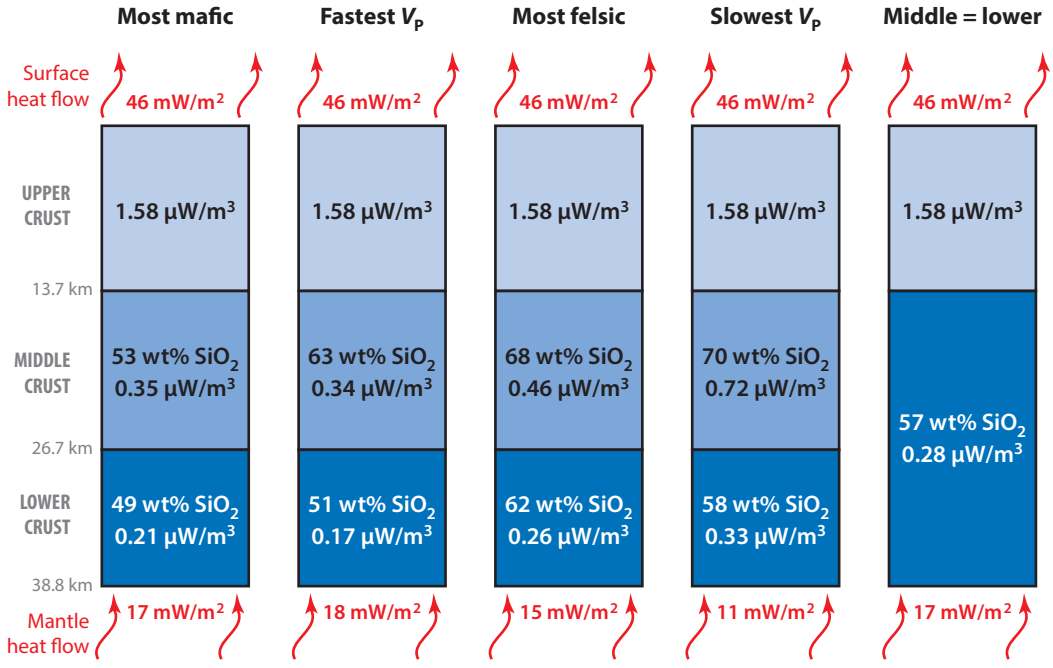

Figure 11

Heat-flow constraints through shields and platforms can be satisfied by a broad range of middle and lower crustal compositions.

lower crust with V_P faster than 7.0 km/s must be as rich in heat-producing elements as the felsic endmember used here. Thus, selecting samples on the basis of seismic wavespeeds yields possible crustal compositions that all have surface heat flow within reasonable bounds for continental crust.

DIFFERENTIATION OF CONTINENTAL CRUST

The origin of continental crust remains enigmatic. The principal conundrum to be resolved is how an andesitic to dacitic continental crust has formed when most mantle-derived magmas are basaltic. As noted above, the similarity in major-element and trace-element composition between bulk continental crust and calc-alkaline arc andesites has led to the widely held hypothesis that continental crust includes a high proportion of arc andesites plus their plutonic equivalents. The fact remains, however, that most primitive arc lavas, with Fe/Mg close to equilibrium with mantle peridotite, are basalts (compilation in Kelemen et al. 2003a, 2014). Further, seismic velocities in arc lower crust are systematically faster than in continental lower crust (Calvert 2011, Hayes et al. 2013). And, the composition of arc lower crust—even after proposed density sorting by

Figure 10

Endmember log-normal average compositions from **Table 4** of (*a*) middle and (*b*) lower continental crust that satisfy V_P and V_P/V_S constraints. (*c*) Resulting bulk continental crust compositions computed as 25 km of middle and lower crust beneath 14 km of the upper crust of Rudnick & Gao (2003, 2014).

delamination[2]—is significantly more depleted in highly incompatible elements compared with continental lower crust (**Figure 3**) (this paper; Kelemen & Behn 2015).

Differentiation of basaltic crust to produce an andesitic crust has been explained as the result of (*i*) weathering (Albarede 1998, Lee et al. 2008, Liu & Rudnick 2011), (*ii*) crust formation from mantle-derived andesitic magmas (Kelemen 1995), (*iii*) mixing of basaltic rock with silicic rock derived by partial melting of mafic, subducting crust (Martin 1986), (*iv*) lower crustal delamination (Arndt & Goldstein 1989, Herzberg et al. 1983, Kay & Kay 1991, Lee 2014, Ringwood & Green 1966), and/or (*v*) relamination (Hacker et al. 2011). Here we contrast the two latter, dynamical processes driven by density variations.

Delamination

To serve as effective differentiation processes, both delamination and relamination require that mantle melting produces differentiated crust in island arcs, and that this raw material is subsequently refined into continental crust. Because most island-arc lavas and plutons are more mafic than continental crust (Kelemen et al. 2003a, 2014), the refining process must selectively return mafic material to the mantle and leave a more-felsic crust behind.

Lower crustal delamination occurs when lower crust and/or underlying mantle lithosphere become gravitationally unstable at temperatures high enough for vertical viscous flow. Igneous processes can lead to delamination if magma intruded into the crust forms a buoyant differentiate that is retained in the crust, plus a dense, ultramafic residue that sinks into the mantle (**Figure 12*a***) (Arndt & Goldstein 1989, Herzberg et al. 1983). Metamorphic processes can also lead to delamination if enough garnet grows in mafic rock (**Figure 12*b***) (Kay & Kay 1991, Ringwood & Green 1966), typically at depths greater than 35 km.

Delamination of 1–10-km-thick layers that are $\leq$300 kg/m^3 denser than mantle can occur at timescales of 1–10 Myr if the Moho temperature is $\geq$900°C (**Figure 13**) (Jagoutz & Behn 2013, Jull & Kelemen 2001). The median amphibolite- and granulite-facies terrain compositions are gravitationally stable with respect to underlying mantle peridotite even at eclogite-facies conditions, whereas the compositions of median granulite xenoliths and many lower crustal rocks in two well-studied island-arc sections are unstable when equilibrated at pressures >1.0–1.5 GPa (i.e., beyond Moho depth in arcs and continents) (**Figure 14**). That a gravitational process acts to density-filter the crust is suggested by the V_P of lower crust, which is a proxy for density. We calculate the relation between density and V_P (after Birch 1961), using two approaches (**Supplemental Figure 4**), and find that the relation is insensitive to temperature in the 300–900°C range. **Figure 7** shows the resulting calculated densities of lower and lowermost crust in different tectonic settings. The average density of lower crust in most tectonic settings is ~3.07 g/cm^3; the average density of the lowermost crust is 3.27 g/cm^3. If upper mantle is considered to have a temperature-dependent density of ~3.25–3.35 g/cm^3 at Moho depths (gray shaded region in **Figure 7**), then nearly all continental crust is buoyant with respect to upper mantle. That said, in shields, platforms, rifts, arcs, and volcanic plateaux, a fraction of lower crust could be denser than upper mantle.

The need for low upper mantle viscosity and density restricts significant lower crustal delamination to warm tectonic settings such as rifts and active arcs (Jull & Kelemen 2001) and

Supplemental Material

[2]We use the term delamination to refer to a family of instabilities in which dense lower crustal lithologies descend into less dense, upper mantle peridotite. Although, for example, the formation of viscous diapirs does not always remove tabular sections of lower crust (i.e., laminae), our use of the term delamination sensu lato to encompass a variety of density instabilities including viscous foundering follows common usage—and is a euphonious complement to relamination.

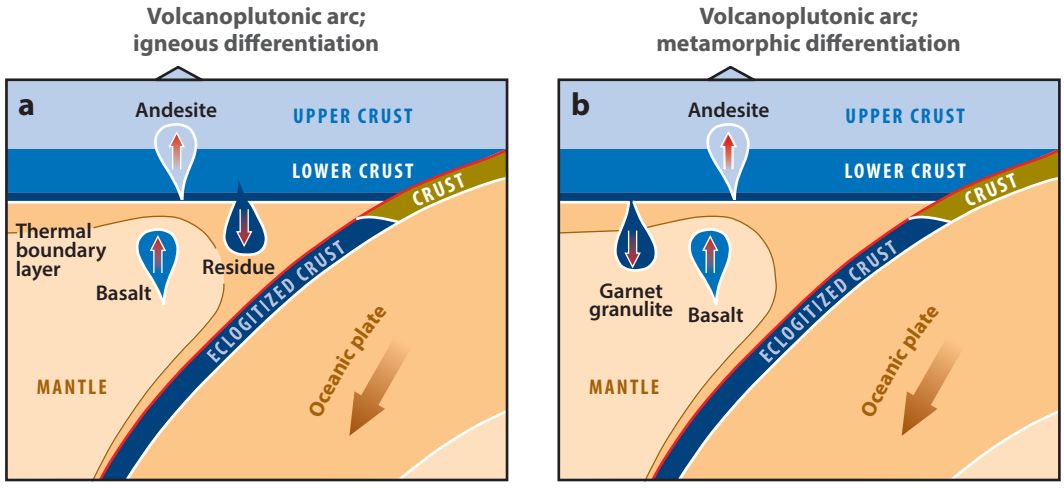

Figure 12

Long-term change in the composition of the continental crust has conventionally been viewed as the result of two major subduction factory processes. (*a*) Mantle-derived magma introduced into volcanoplutonic arcs differentiates into an andesitic fraction that is retained in the crust and an ultramafic cumulate that becomes part of the mantle (Arndt & Goldstein 1989). (*b*) Mafic rock at the base of a thick volcanoplutonic arc is converted into garnet granulite and sinks into the mantle (Herzberg et al. 1983).

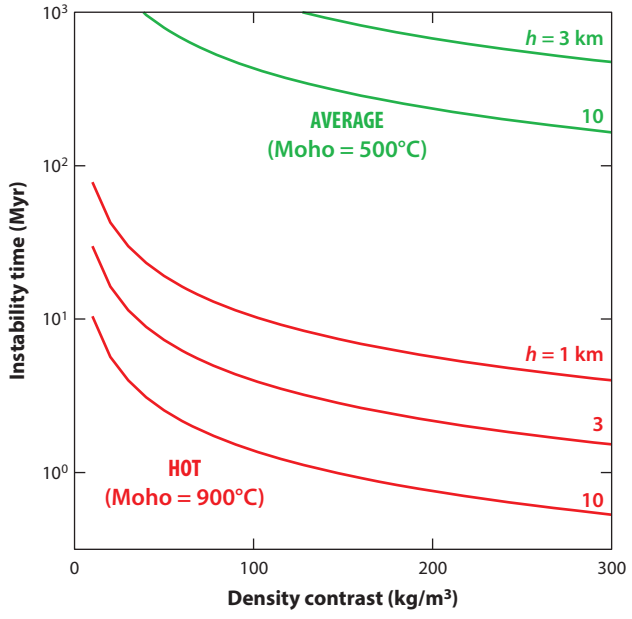

Figure 13

Gravitationally unstable layers 1–10 km thick can delaminate at Moho temperatures of 900°C on a 1–10-Myr timescale.

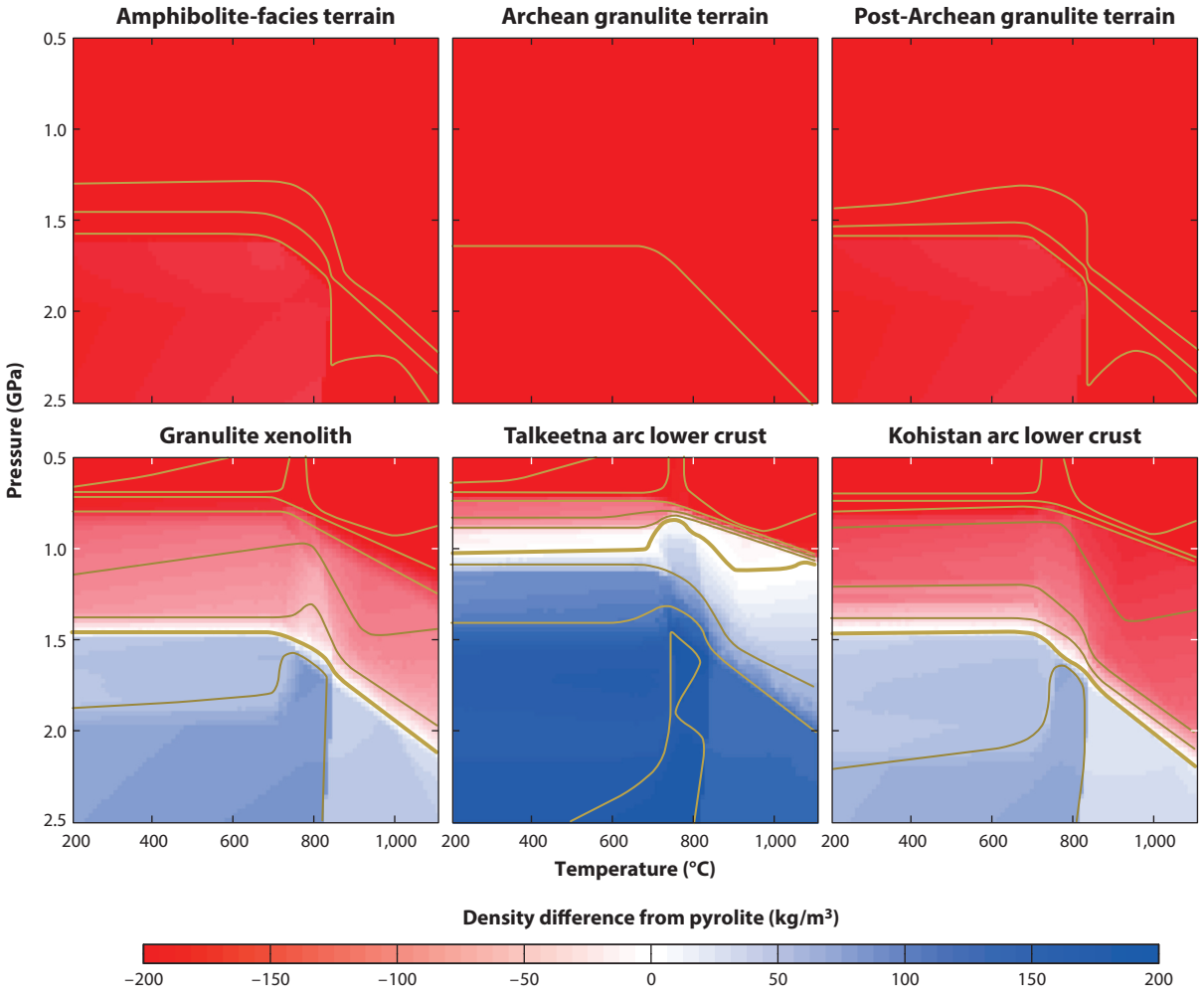

Figure 14

Calculated densities of median lower crustal lithologies relative to pyrolite mantle. Median amphibolite- and granulite-facies terrain compositions are gravitationally stable at all modeled pressures, whereas the median granulite-facies xenolith and arc lower crust compositions are unstable at $P > 1$–1.5 GPa and $T \geq 800$°C. Calculations were done with Perple_X for 0.5 wt% H_2O and mineralogy held constant for $T \leq 700$°C; melting was not included.

perhaps continent collision zones; the presence of a dense, ultramafic lowermost crust and/or garnet-rich metamorphic rocks below 35 km in such settings (**Figure 7*c*,*d***) may, therefore, be ephemeral (**Figure 13**).

The upper mantle beneath shields and platforms and beneath orogens is likely too cold to permit development of a convective instability (**Figure 13**). The presence of a high-V_P lower crust beneath some shields and platforms (**Figure 7*a***)—and the absence of a high-V_P lower crust in Paleozoic–Mesozoic orogens (**Figure 7*b***)—suggests that underplating of mantle-generated, mafic melts may have occurred beneath some shields and platforms (Korja & Heikkinen 1995; Rudnick & Gao 2003, 2014) or that slow recrystallization and formation of metamorphic garnet

gradually increases wavespeeds over time (Fischer 2002) in areas where the base of the crust is too cold and viscous to undergo convective instability on geologically relevant timescales.

Relamination

Though delamination of dense lower crust probably is recorded in some arc sections (Behn & Kelemen 2006, DeBari & Sleep 1991, Ducea & Saleeby 1996, Kay & Kay 1988, Kelemen et al. 2003a), with the exception of the Kohistan arc (Jagoutz & Behn 2013), the remaining arc lower crust after delamination is very different from continental lower crust (**Figure 3**) (DeBari & Sleep 1991, Greene et al. 2006, Kelemen & Behn 2015). Garnet-free mafic rocks are gravitationally stable, and dense ultramafic rocks may be retained where temperatures are too low for viscous instabilities. Other tectonic processes that can aid in the refining of continental crust are therefore required to explain the transformation of arc crust to continental crust. Hacker et al. (2011) suggested relamination as another major refining process.

Relamination is a corollary process to delamination, in which buoyant, felsic crustal material is subducted, separated from the downgoing plate, and returned to the upper plate crust (Hacker et al. 2011) while denser, mafic material is transformed into eclogite and descends further into the mantle. The many forms of relamination are potentially important because they provide another mechanism by which (*i*) felsic material is introduced into lower crust, (*ii*) gravitationally unstable mafic rock can be removed from the crust, and (*iii*) low-density volatiles and melt can separate to rise into middle or upper crust, leaving a denser residuum in lower crust. This process will be most efficient in arcs where upper mantle temperatures are sufficiently high at the base of the crust (Kelemen et al. 2003b) to permit vertical viscous flow due to buoyancy of the felsic fraction (Behn et al. 2011, Kelemen & Behn 2015).

Relamination is envisaged to occur during four subduction-zone processes (**Figure 15**): (*i*) sediment subduction, (*ii*) arc subduction, (*iii*) forearc subduction or subduction erosion, and (*iv*) continent subduction (Hacker et al. 2011). The relamination process can take the form of imbrication of material beneath the upper plate crust (Kimbrough & Grove 2007), buoyant ascent from mantle depths to the base of the crust along a subduction channel (Gerya et al. 2008, Li & Gerya 2009, Warren et al. 2008), and/or ascent of buoyant diapirs through the mantle wedge to the base of the crust (Behn et al. 2011, Currie et al. 2007, Gerya & Meilick 2011, Gerya & Yuen 2003, Gorczyk et al. 2006, Kelemen et al. 2003a, Yin et al. 2007, Zhu et al. 2009). In all of these processes, other than imbrication, all of the subducting material is carried to eclogite-facies conditions. This is in contrast to delamination of mafic rocks, which requires garnet growth at depths greater than ~30–35 km and thus only occurs near the base of the crust.

For this reason, relamination is more efficient than delamination in distilling a dominantly felsic crust. Kelemen & Behn (2015) demonstrated that arc crustal components more buoyant than mantle peridotite at eclogite-facies conditions have major- and trace-element compositions within the range of estimated lower continental crust (**Figure 3**). Thus, this process can create large volumes of lower continental crust by relaminating the base of the crust with buoyant felsic rocks and purging the crust of eclogitized mafic rocks, dense cumulates produced by crystal fractionation, and dense residues of crustal partial melting (Kelemen & Behn 2015).

Cenozoic rates of sediment subduction, forearc subduction, arc subduction, and continent subduction total approximately 3.4–4.5 km^3/yr; the densities of subducted materials in eclogite facies suggest that 2.1–2.9 km^3/yr (60–65%) may be relaminated (Hacker et al. 2011). A similar estimate has been made from the bulk $\delta^{18}O$ value for the continental crust (Simon & Lécuyer 2005).

In contrast, Kramers & Tolstikhin's (1997) future Pb paradox, which was based on a secular increase in crustal recycling rate, requires that 60% of new crustal material is currently being

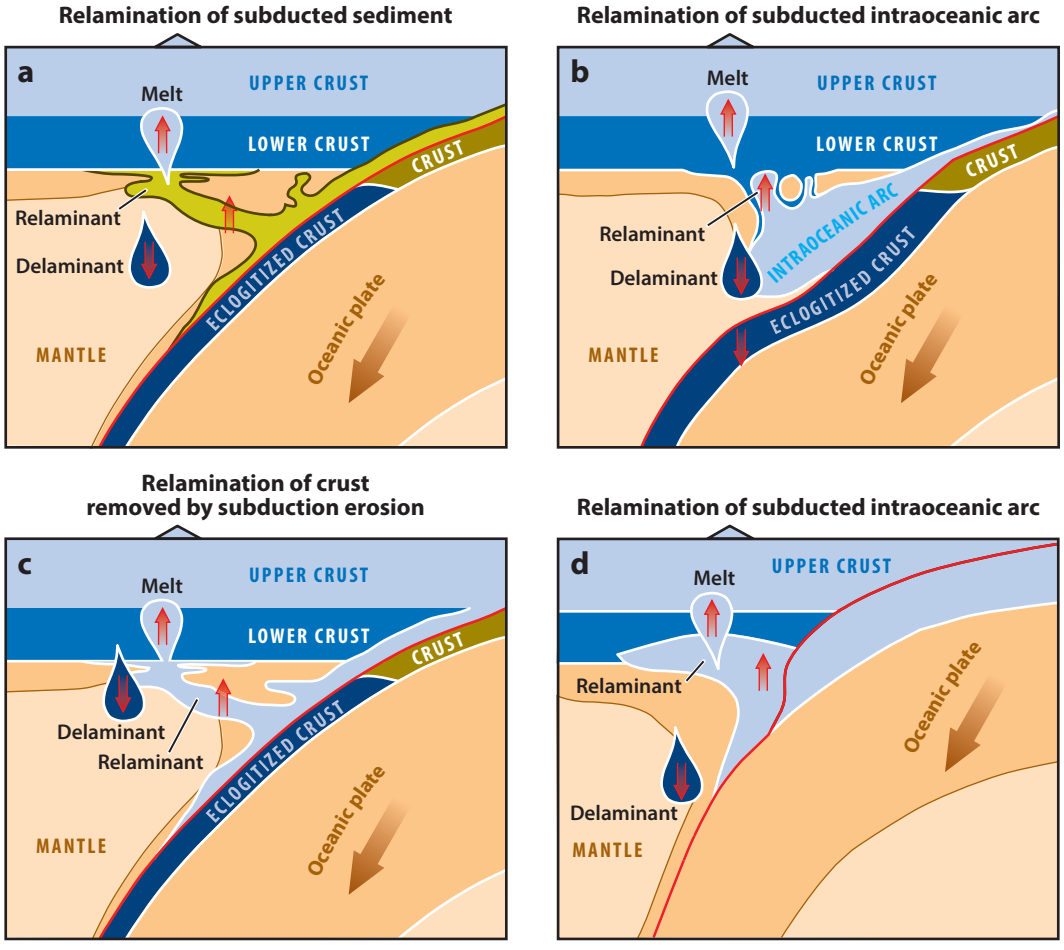

Figure 15

Four tectonic settings for continental refining via relamination. In all cases, depending on physical conditions, the relaminating layer may be thrust directly beneath existing crust; rise en bloc, perhaps in a subduction channel; or rise as diapirs through the mantle wedge. In all cases, there may be melting that produces a liquid that ascends well above the relaminating layer, and there may be residues that are either positively or negatively buoyant with respect to the adjacent mantle. (*a*) Subducted sediment is thrust into or beneath arc lower crust or is gravitationally unstable and rises to relaminate the base of the crust in the upper plate. (*b*) Subducted volcanoplutonic arcs undergo density separation as mafic lower crust transforms to eclogite while buoyant upper crust relaminates the base of the crust in the upper plate. (*c*) Felsic crustal material removed from the upper plate by subduction erosion is relaminated to the base of the crust in the upper plate; mafic material transforms to eclogite and sinks within upper mantle. (*d*) Subducted felsic continental crust is relaminated to the base of the crust in the upper plate. Any (ultra)mafic material of sufficient size transforms to eclogite and returns to upper mantle.

recycled into Earth's mantle. Similarly, Scholl & von Huene (2007) estimated that 95% of subducted sediment is returned to the mantle. Because of the likelihood of relamination, for subducting, buoyant sedimentary layers more than ~100 m thick (Behn et al. 2011) this estimate may be far too large (Hacker et al. 2011).

Relamination Examples

There are several possible examples of relamination. The first suggested case of relamination of the felsic section of a subducting arc (**Figure 15*b***) comes from the Izu–Bonin–Mariana arc collision with the Honshu arc. The Honshu arc is intruded by intermediate to felsic rocks (Tanzawa tonalites and Kofu granitic complex) that are interpreted as part of the subducted Izu–Bonin–Mariana arc that partially melted and was relaminated (Tamura et al. 2010). Relamination of the felsic section of a subducting continent (**Figure 15*d***) was suggested by Chemenda et al. (2000), who proposed that the subducted upper crust of India is being relaminated to form lower crust of Tibet. The ultrahigh-temperature and ultrahigh-pressure crust of the Bohemian Massif (and perhaps much of the Variscan of Europe) is interpreted to be a felsic crustal layer that was relaminated beneath a denser layer and then rose as a gravitational instability (Guy et al. 2011, Lexa et al. 2011). Two excellent examples of relaminated sediment (**Figure 15*a***) are (*i*) the Pelona-type schists that underlie much of southern California, which are underthrust sediment derived by erosion of the overlying magmatic arc (Jacobson et al. 2011), and (*ii*) the Triassic flysch that was thrust beneath the central part of Tibet during the Jurassic (Kapp et al. 2003). The Pliocene ultrahigh-pressure rocks in Papua New Guinea, which are composed largely of Cretaceous volcanic rocks (Zirakparvar et al. 2012), may be a third example. The North Qaidam ultrahigh-pressure terranes of central China and the Penninic Alps have been proposed to be amalgams of relaminated material removed by subduction erosion (**Figure 15*a***) (Stöckhert & Gerya 2005, Yin et al. 2007). Relamination has also been produced in multiple analytical and computational models (Behn et al. 2011, Gerya & Meilick 2011, Vogt et al. 2013, Yin et al. 2007).

REVISITING THE BULK COMPOSITION OF CONTINENTAL CRUST

Table 4 provides a set of endmember compositions for the lower and middle crust (mafic and felsic, high and low V_P) derived from the approach presented in **Figures 8** and **9**. It also includes corresponding bulk crust compositions using these endmembers together with a 14-km-thick upper crust with the composition given by Rudnick & Gao (2003, 2014) to produce a 39-km-thick crust appropriate for shields, platforms, and orogens (**Table 1**). The likely SiO_2 content of lower crust ranges from 49 to 62 wt% SiO_2, and likely middle crust estimates range from 53 to 70 wt% SiO_2; these yield a corresponding range of bulk crustal compositions with 56–65 wt% SiO_2.

For the more-felsic lower crust compositions, the concentrations of K, P, LREEs, and other highly to moderately incompatible trace elements differ from the lower crustal estimates of Rudnick & Gao (2003, 2014), in many cases by a factor of two or more. Our middle crust estimates are systematically depleted in incompatible trace elements compared with those of Rudnick & Gao (2003, 2014). For bulk crust, there is little difference between our estimates and the bulk crust composition estimates of Rudnick & Gao (2003, 2014).

As in the model adopted in most recent studies of continental crust, the mafic, median composition of continental granulite xenoliths remains a potentially significant component in lowermost continental crust. However, although this component is commonly treated as though it is similar to arc lower crust (e.g., Jagoutz & Schmidt 2012) and represents a residual or cumulate composition complementary to the more-felsic upper crust, in fact the origin of the granulite xenolith component is not simple to understand. First, it is not geochemically similar to arc lower crust (see **Figure 3** and the associated text). Second, other than a marked depletion in U and Th and high Eu/Sm (indicative of residual or accumulated plagioclase), the granulite xenolith component has trace-element characteristics that are roughly parallel to those of continental crust, similar to LREE-enriched, HREE-depleted basaltic lavas in arcs such as the Aleutians

(e.g., figure 1 in Kelemen & Dunn 1993), and different from mafic cumulates produced by crystal fractionation of basalt in arcs. Perhaps the median granulite xenolith composition represents the mafic residue of (*i*) differentiation of andesitic magma in the crust, (*ii*) partial melting of relaminating lithologies with an andesitic composition, and/or (*iii*) assimilation of (relaminated) lower crustal metasediments in basaltic lava, after extraction and ascent of evolved melt. The major elements in all three of these scenarios are well modeled by the experiments of Patiño Douce (1995) at 1,000°C and 0.5–1.5 GPa, with SiO_2 contents of 56 wt% in the bulk composition, 70–74 wt% in melts, and 50–51 wt% in residues. If residues of such processes include trace element–rich minor phases, such as monazite and/or allanite, so that bulk distribution coefficients were ~1, the residues might resemble the median granulite xenolith composition.

Most importantly, the majority of continental lower crust, with V_P from 6.7 to 7.3 km/s, may or may not be mafic and could have SiO_2 contents up to 62 wt%. Some continental lower crust, with V_P less than 6.7 km/s, almost certainly has an andesitic to dacitic bulk composition with more than 55 wt% SiO_2. Thus, large proportions of continental lower crust could have a composition similar to that of amphibolite- and granulite-facies metamorphic terrains. Furthermore, lower and middle crust might be compositionally equivalent. The possible, relatively felsic compositions for lower continental crust in **Table 4** resemble most older estimates for lower continental crust (e.g., Weaver & Tarney 1984), based on the composition of high-grade metamorphic terrains.

In summary, the new estimates of lower, middle, and bulk continental crust composition presented here satisfy seismic wavespeed constraints for individual rocks and a range of mantle and surface heat-flow values. The new estimates range from values close to those of Rudnick & Gao (2003, 2014) to significantly more-felsic compositions that hark back to the earlier literature on continental crust.

SUMMARY POINTS

1. Continental crust is on average 34 km thick, but shields, platforms, and Paleozoic–Mesozoic orogens and their contiguous continental shelves—which make up ~70% by area—are 39–40 km thick.
2. Most lower crust could have SiO_2 contents between ~49 and 62 wt%, with high to moderate concentrations of K, Th, and U, on the basis of heat flow, wavespeeds, and representative rock compositions.
3. Portions of crust with $V_P > 7.2$ km/s must be mafic. Approximately 20% of lower crust (2.4 km) has wavespeeds this fast.
4. Beneath shields and platforms, V_P suggests that 20–30% of lower crust is mafic. A large fraction of this material could be denser than peridotite. In these settings the underlying upper mantle is too cold to permit development of a convective instability. High-V_P lithologies in these settings may be the result of mafic underplating or of slow metamorphic growth of large proportions of garnet.
5. V_P values from lower crust of Paleozoic–Mesozoic orogens indicate a smaller amount of mafic rock and little or no material that is denser than peridotite.
6. Beneath rifts, arcs, and volcanic plateaux and beneath continent collision zones, ~10–20% of lower crust is mafic, and about half that is denser than peridotite. The inferred gravitational instability and high Moho temperatures suggest that the mafic lower crust in these regions may be temporary.

7. Relamination is a potentially important mechanism by which buoyant crustal material can be transformed into lower crust. In convergence zones, mafic rocks are dense enough to sink within mantle, whereas felsic rocks are positively buoyant and can relaminate the base of the upper plate crust. This can take place during sediment subduction, subduction erosion, subduction of arc crust, and subduction of continental crust. Estimated mass fluxes for these processes are sufficiently large that they could have refined the composition of the entire continental crust over the lifetime of Earth, leading to the present composition of the crust in many regions.

DISCLOSURE STATEMENT

The authors are not aware of any affiliations, memberships, funding, or financial holdings that might be perceived as affecting the objectivity of this review.

ACKNOWLEDGMENTS

When we began this study, Roberta Rudnick graciously provided an updated database of post-Archean granulite terrain compositions and lower-crustal xenolith compositions, supplementing the landmark study by Rudnick & Presper (1990). Roberta also selflessly reviewed this manuscript, as did Geoff Abers and an anonymous Annual Reviews editor. Brian Evans, Greg Hirth, and Ian Jackson provided helpful insight into interpreting the elastic behavior of quartz at high *P* and *T*. This material is based upon work supported by National Science Foundation grants EAR-1049905, OCE-1144759, EAR-1219942, EAR-1249703, and EAR-1316333.

LITERATURE CITED

Albarede F. 1998. The growth of continental crust. *Tectonophysics* 296:1–14

Arndt NT, Goldstein SL. 1989. An open boundary between lower continental crust and mantle: its role in crust formation and crustal recycling. *Tectonophysics* 161:201–12

Babeyko AY, Sobolev SV, Sinelnikov ED, Smirnov YP, Derevschikova NA. 1994. Calculation of elastic properties in lower part of the Kola borehole from bulk chemical compositions of core samples. *Surv. Geophys.* 15:545–73

Barker F, Peterman ZE. 1974. Bimodal tholeiitic-dacitic magmatism and the early Precambrian crust. *Precambrian Res.* 1:1–12

Bassin C, Laske G, Masters G. 2000. The current limits of resolution for surface wave tomography in North America. *Eos Trans. AGU* 81:F897

Behn MD, Kelemen PB. 2003. Relationship between seismic P-wave velocity and the composition of anhydrous igneous and meta-igneous rocks. *Geochem. Geophys. Geosyst.* 4:1041

Behn MD, Kelemen PB. 2006. The stability of arc lower crust: insights from the Talkeetna arc section, south-central Alaska and the seismic structure of modern arcs. *J. Geophys. Res.* 111:B11207

Behn MD, Kelemen PB, Hirth G, Hacker BR, Massonne HJ. 2011. Diapirs as the source of the sediment signature in arc lavas. *Nat. Geosci.* 4:641–46

Birch F. 1961. The velocity of compressional waves in rocks to 10 kilobars: 2. *J. Geophys. Res.* 66:2199–224

Bond CE, Gibbs AD, Shipton ZK, Jones S. 2007. What do you think this is? "Conceptual uncertainty" in geoscience interpretation. *GSA Today* 17:4–10

Calvert AJ. 2011. The seismic structure of island arc crust. In *Arc-Continent Collision*, ed. D Brown, PD Ryan, pp. 87–119. Berlin: Springer-Verlag

Chemenda AI, Burg JP, Mattauer M. 2000. Evolutionary model of the Himalaya–Tibet system: geopoem: based on new modelling, geological and geophysical data. *Earth Planet. Sci. Lett.* 174:397–409

Christensen NI. 1989. Reflectivity and seismic properties of the deep continental crust. *J. Geophys. Res.* 94(B12):17793–804

Christensen NI. 1996. Poisson's ratio and crustal seismology. *J. Geophys. Res.* 101(B2):3139–56

Christensen NI, Mooney WD. 1995. Seismic velocity structure and composition of the continental crust: a global view. *J. Geophys. Res.* 100(B6):9761–88

Currie CA, Beaumont C, Huismans RS. 2007. The fate of subducted sediments: a case for backarc intrusion and underplating. *Geology* 35:1111–14

DeBari SM, Sleep NH. 1991. High-Mg, low-Al bulk composition of the Talkeetna island arc, Alaska: implications for primary magmas and the nature of arc crust. *Geol. Soc. Am. Bull.* 103:37–47

Ducea MN, Saleeby JB. 1996. Buoyancy sources for a large unrooted mountain range, the Sierra Nevada, California: evidence from xenolith thermobarometry. *J. Geophys. Res.* 101(B4):8229–41

Fischer K. 2002. Waning buoyancy in the crustal roots of old mountains. *Nature* 417:933–36

Fountain DM, Arculus R, Kay RW, eds. 1992. *Continental Lower Crust*. Amsterdam: Elsevier

Fountain DM, Salisbury MH. 1981. Exposed cross-sections through the continental crust: implications for crustal structures, petrology and evolution. *Earth Planet. Sci. Lett.* 56:267–77

Gao S, Luo TC, Zhang BR, Zhang HF, Han YW, et al. 1998. Chemical composition of the continental crust as revealed by studies in East China. *Geochim. Cosmochim. Acta* 62:1959–75

Gerya TV, Meilick FI. 2011. Geodynamic regimes of subduction under an active margin: effects of rheological weakening by fluids and melts. *J. Metamorph. Geol.* 29:7–31

Gerya TV, Perchuk LL, Burg JP. 2008. Transient hot channels: perpetrating and regurgitating ultrahigh-pressure, high temperature crust-mantle associations in collision belts. *Lithos* 103:236–56

Gerya TV, Yuen DA. 2003. Rayleigh–Taylor instabilities from hydration and melting propel 'cold plumes' at subduction zones. *Earth Planet. Sci. Lett.* 212:47–62

Gorczyk W, Gerya TV, Connolly JAD, Yuen DA, Rudolph M. 2006. Large-scale rigid-body rotation in the mantle wedge and its implications for seismic tomography. *Geochem. Geophys. Geosyst.* 7:Q05018

Greene AR, DeBari SM, Kelemen PB, Blusztajn J, Clift PD. 2006. A detailed geochemical study of island arc crust: the Talkeetna Arc section, south-central Alaska. *J. Petrol.* 47:1051–93

Guy A, Edel JB, Schulmann K, Tomek Č, Lexa O. 2011. A geophysical model of the Variscan orogenic root (Bohemian Massif): implications for modern collisional orogens. *Lithos* 124:144–57

Hacker BR, Kelemen PB, Behn MD. 2011. Differentiation of the continental crust by relamination. *Earth Planet. Sci. Lett.* 307:501–16

Halliday AN, Dickin AP, Hunter RN, Davies GR, Dempster TJ, et al. 1993. Formation and composition of the lower continental crust: evidence from Scottish xenolith suites. *J. Geophys. Res.* 98(B1):581–607

Hayes JL, Holbrook WS, Lizarralde D, van Avendonk HJA, Bullock AD, et al. 2013. Crustal structure across the Costa Rican Volcanic Arc. *Geochem. Geophys. Geosyst.* 14:1087–103

Heier KS, Adams JAS. 1965. Concentration of radioactive elements in deep crustal material. *Geochim. Cosmochim. Acta* 29:53–61

Herzberg CT, Fyfe WS, Carr MJ. 1983. Density constraints on the formation of the continental Moho and crust. *Contrib. Mineral. Petrol.* 84:1–5

Holbrook WS, Mooney WD, Christensen NI. 1992. The seismic velocity structure of the deep continental crust. See Fountain et al. 1992, pp. 1–42

Holland HD, Turekian KK, eds. 2003. *Treatise on Geochemistry*, Vol. 3: *The Crust*. Oxford, UK: Elsevier-Pergamon. 1st ed.

Holland HD, Turekian KK, eds. 2014. *Treatise on Geochemistry*, Vol. 4: *The Crust*. Oxford, UK: Elsevier-Pergamon. 2nd ed.

Huang Y, Chubakov V, Mantovani F, Rudnick RL, McDonough WF. 2013. A reference Earth model for the heat-producing elements and associated geoneutrino flux. *Geochem. Geophys. Geosyst.* 14:2003–29

Jacobson CE, Grove M, Pedrick JN, Barth AP, Marsaglia KM, et al. 2011. Late Cretaceous–early Cenozoic tectonic evolution of the southern California margin inferred from provenance of trench and forearc sediments. *Geol. Soc. Am. Bull.* 123:485–506

Jagoutz O, Behn MD. 2013. Foundering of lower island-arc crust as an explanation for the origin of the continental Moho. *Nature* 504:131–34

Jagoutz O, Schmidt MW. 2012. The formation and bulk composition of modern juvenile continental crust: the Kohistan arc. *Chem. Geol.* 298–99:79–96

Jaupart C, Mareschal JC. 2003. Constraints on crustal heat production from heat flow data. See Holland & Turekian 2003, pp. 65–84

Jordan EK, Lieu W, Stern RJ, Carr MJ, Feigenson MD, Gill JB. 2012. *CentAm & IBM Geochem Database*, version 1.02. Palisades, NY: Integr. Earth Data Appl. **http://www.iedadata.org/doi?id=100053**

Jull M, Kelemen PB. 2001. On the conditions for lower crustal convective instability. *J. Geophys. Res.* 106(B4):6423–45

Kapp P, Yin A, Manning CE, Harrison TM, Taylor MH, Ding L. 2003. Tectonic evolution of the early Mesozoic blueschist-bearing Qiangtang metamorphic belt, central Tibet. *Tectonics* 22:1043

Kay RW, Kay SM. 1988. Crustal recycling and the Aleutian arc. *Geochim. Cosmochim. Acta* 52:1351–59

Kay RW, Kay SM. 1991. Creation and destruction of lower continental crust. *Geol. Rundsch.* 80:259–78

Kelemen P. 1995. Genesis of high Mg# andesites and the continental crust. *Contrib. Mineral. Petrol.* 120:1–19

Kelemen P, Behn MD. 2015. Relamination not delamination: Lower continental crust forms via arc magmatism followed by underplating of subducted, buoyant arc lavas and plutons. *Nat. Geosci.* In press

Kelemen PB, Dunn NST. 1993. Relative depletion of niobium in some arc magmas and the continental crust: partitioning of K, Nb, La and Ce during melt/rock reaction in the upper mantle. *Earth Planet. Sci. Lett.* 120:111–34

Kelemen PB, Hanghøj K, Greene A. 2003a. One view of the geochemistry of subduction-related magmatic arcs, with an emphasis on primitive andesite and lower crust. See Holland & Turekian 2003, pp. 593–659

Kelemen PB, Hanghøj K, Greene A. 2014. One view of the geochemistry of subduction-related magmatic arcs, with an emphasis on primitive andesite and lower crust. See Holland & Turekian 2014, pp. 749–806

Kelemen PB, Parmentier EM, Rilling J, Mehl L, Hacker BR. 2003b. Thermal structure due to solid-state flow in the mantle wedge beneath arcs. *AGU Monogr.* 138:293–311

Kern H, Gao S, Liu QS. 1996. Seismic properties and densities of middle and lower crustal rocks exposed along the North China Geoscience Transect. *Earth Planet. Sci. Lett.* 139:439–55

Kimbrough DL, Grove M. 2007. Evidence for rapid recycling of subduction erosion forearc material into Cordilleran TTG batholiths: insight from the Peninsular Ranges of southern and Baja California. *Eos Trans. AGU* 88(Fall Meet. Suppl.):T11B-0581 (Abstr.)

Korja A, Heikkinen PJ. 1995. Proterozoic extensional tectonics of the central Fennoscandian Shield: results from the Baltic and Bothnian Echoes from the Lithosphere experiment. *Tectonics* 14:504–17

Kramers JD, Tolstikhin IN. 1997. Two terrestrial lead isotope paradoxes, forward transport modelling, core formation and the history of the continental crust. *Chem. Geol.* 139:75–100

Lambert IB, Heier KS. 1968. Geochemical investigations of deep-seated rocks in the Australian Shield. *Lithos* 1:30–53

Laske G, Masters G, Ma Z, Pasyanos M. 2013. Update on CRUST1.0: a 1-degree global model of Earth's crust. *Geophys. Res. Abstr.* 15:EGU2013–658

Lee CTA. 2014. Physics and chemistry of continental crust recycling. See Holland & Turekian 214, pp. 423–56

Lee CTA, Morton DM, Little MG, Kistler R, Horodyskyj UN, et al. 2008. Regulating continent growth and composition by chemical weathering. *PNAS* 105:4981–86

Lexa O, Schulmann K, Janoušek V, Štípská P, Guy A, Racek M. 2011. Heat sources and trigger mechanisms of exhumation of HP granulites in Variscan orogenic root. *J. Metamorph. Geol.* 29:79–102

Li Z, Gerya TV. 2009. Polyphase formation and exhumation of high- to ultrahigh-pressure rocks in continental subduction zone: numerical modeling and application to the Sulu ultrahigh-pressure terrane in eastern China. *J. Geophys. Res.* 114:B09406

Liu XM, Rudnick RL. 2011. Constraints on continental crustal mass loss via chemical weathering using lithium and its isotopes. *PNAS* 108:20873–80

Martin H. 1986. Effect of steeper Archean geothermal gradient on geochemistry of subduction-zone magmas. *Geology* 14:753–56

McLennan SM, Taylor SR, Heming SR. 2005. Composition, differentiation, and evolution of continental crust: constraints from sedimentary rocks and heatflow. In *Evolution and Differentiation of the Continental Crust*, ed. M Brown, T Rushmer, pp. 92–134. Cambridge, UK: Cambridge Univ. Press

Michaut C, Jaupart C, Mareschal JC. 2009. Thermal evolution of cratonic roots. *Lithos* 109:47–60
Miller DJ, Christensen NI. 1994. Seismic signature and geochemistry of an island arc: a multidisciplinary study of the Kohistan accreted terrane, northern Pakistan. *J. Geophys. Res.* 99(B6):11623–42
Mooney WD, Laske G, Master TG. 1998. CRUST 5.1: a global crustal model at 5° × 5°. *J. Geophys. Res.* 103(B1):727–47
Morgan P, Sawka WN, Furlong KP. 1987. Introduction: background and implications of the linear heat flow-heat production relationship. *Geophys. Res. Abstr.* 14:248–51
Musacchio G, Mooney WD, Luetgert JH, Christensen NI. 1997. Composition of the crust in the Grenville and Appalachian Provinces of North America inferred from *VP/VS* ratios. *J. Geophys. Res.* 102(B7):15225–41
Pakiser LC, Robinson R. 1966. Composition and evolution of the continental crust as suggested by seismic observations. *Tectonophysics* 3:547–57
Patiño Douce AE. 1995. Experimental generation of hybrid silicic melts by reaction of high-Al basalt with metamorphic rocks. *J. Geophys. Res.* 100(B8):15623–39
Percival JA, Fountain DM, Salisbury M. 1992. Exposed crustal cross sections as windows on the lower crust. See Fountain et al. 1992, pp. 317–62
Reid MR, Hart SR, Padovani ER, Wandless GA. 1989. Contribution of metapelitic sediments to the composition, heat production, and seismic velocity of the lower crust of southern New Mexico, U.S.A. *Earth Planet. Sci. Lett.* 95:367–81
Ringwood AE, Green DH. 1966. An experimental investigation of the gabbro-eclogite transformation and some geophysical implications. *Tectonophysics* 3:383–427
Rudnick RL. 1992. Xenoliths—samples of the lower continental crust. See Fountain et al.. 1992, pp. 269–316
Rudnick RL, Fountain DM. 1995. Nature and composition of the continental crust: a lower crustal perspective. *Rev. Geophys.* 33:267–309
Rudnick RL, Gao S. 2003. Composition of the continental crust. See Holland & Turekian 2003, pp. 1–64
Rudnick RL, Gao S. 2014. Composition of the continental crust. See Holland & Turekian 2014, pp. 1–51
Rudnick RL, Goldstein SL. 1990. The Pb isotopic compositions of lower crustal xenoliths and the evolution of lower crustal Pb. *Earth Planet. Sci. Lett.* 98:192–207
Rudnick RL, Presper T. 1990. Geochemistry of intermediate- to high-pressure granulites. *NATO Sci. Ser. C* 311:523–50
Scholl DW, von Huene R. 2007. Crustal recycling at modern subduction zones applied to the past—issues of growth and preservation of continental basement, mantle geochemistry, and supercontinent reconstruction. *Geol. Soc. Am. Mem.* 200:9–32
Shaw DM, Reilly GA, Muysson JR, Pattenden GE, Campbell AF. 1967. An estimate of the chemical composition of the Canadian Precambrian shield. *Can. J. Earth Sci.* 4:829–53
Simon L, Lécuyer C. 2005. Continental recycling: the oxygen isotope point of view. *Geochem. Geophys. Geosyst.* 6:Q08004
Singer BS, Jicha BR, Leeman WP, Rogers NW, Thirlwall MF, et al. 2007. Along-strike trace element and isotopic variation in Aleutian Island arc basalt: subduction melts sediments and dehydrates serpentine. *J. Geophys. Res.* 112:B06206
Smithson SB. 1978. Modeling continental crust: structural and chemical constraints. *Geophys. Res. Lett.* 5:749–52
Sobolev SV, Babeyko AY. 1994. Modeling of mineralogical composition, density and elastic-wave velocities in anhydrous magmatic rocks. *Surv. Geophys.* 15:515–44
Stöckhert B, Gerya TV. 2005. Pre-collisional high pressure metamorphism and nappe tectonics at active continental margins: a numerical simulation. *Terra Nova* 17:102–10
Su YJ. 2002. *Mid-ocean ridge basalt trace element systematics: constraints from database management, ICPMS analyses, global data compilation, and petrologic modeling*. PhD Thesis, Columbia Univ., New York, NY
Tamura Y, Ishizuka O, Aoike K, Kawate S, Kawabata H, et al. 2010. Missing Oligocene crust of the Izu–Bonin arc: consumed or rejuvenated during collision? *J. Petrol.* 51:823–46
Taylor SR. 1967. The origin and growth of continents. *Tectonophysics* 4:17–34
Tredoux M, Hart RJ, Carlson RW, Shirey SB. 1999. Ultramafic rocks at the center of the Vredefort structure: further evidence for the crust on edge model. *Geology* 27:923–26

Vogt K, Castro A, Gerya T. 2013. Numerical modeling of geochemical variations caused by crustal relamination. *Geochem. Geophys. Geosyst.* 14:470–87

Wanless VD, Perfit MR, Ridley WI, Klein E. 2010. Dacite petrogenesis on mid-ocean ridges: evidence for oceanic crustal melting and assimilation. *J. Petrol.* 51:2377–410

Warren CJ, Beaumont C, Jamieson RA. 2008. Modelling tectonic styles and ultra-high pressure (UHP) rock exhumation during the transition from oceanic subduction to continental collision. *Earth Planet. Sci. Lett.* 267:129–45

Weaver BL, Tarney J. 1984. Empirical approach to estimating the composition of the continental crust. *Nature* 310:575–77

Yin A, Manning CE, Lovera O, Menold CA, Chen X, Gehrels GE. 2007. Early Paleozoic tectonic and thermomechanical evolution of ultrahigh-pressure (UHP) metamorphic rocks in the northern Tibetan Plateau, northwest China. *Int. Geol. Rev.* 49:681–716

Yogodzinski GM, Brown ST, Kelemen P, Vervoort J, Portnya M, et al. 2015. The role of subducted basalt in the source of island arc magmas: evidence from seafloor lavas of the western Aleutians. *J. Petrol.* In press

Zhu G, Gerya TV, Yuen DA, Honda S, Yoshida T, Connolly JAD. 2009. Three-dimensional dynamics of hydrous thermal-chemical plumes in oceanic subduction zones. *Geochem. Geophys. Geosyst.* 10:Q11006

Zirakparvar NA, Baldwin SL, Vervoort JD. 2012. The origin and geochemical evolution of the Woodlark Rift of Papua New Guinea. *Gondwana Res.* 23:931–43